

Intrinsic Mixed-state Quantum Topological Order

Zijian Wang,^{1,*} Zhengzhi Wu,^{1,*} and Zhong Wang^{1,†}

¹*Institute for Advanced Study, Tsinghua University, Beijing 100084, People's Republic of China*

Decoherence is a major obstacle to the preparation of topological order in noisy intermediate-scale quantum devices. Here, we show that decoherence can also give rise to new types of topological order. Specifically, we construct concrete examples by proliferating fermionic anyons in the toric code via local quantum channels. The resulting mixed states retain long-range entanglement, which manifests in the nonzero topological entanglement negativity, though the topological quantum memory is destroyed by decoherence. By comparison to the gapless spin liquid in pure states, we show that the identified states represent a novel intrinsic mixed-state quantum topological order, which has no counterpart in pure states. Through the lens of quantum anomalies of 1-form symmetries, we then provide general constructions of intrinsic mixed-state quantum topological order, and reveal the existence of non-bosonic deconfined anyons as another key feature of these novel phases. The extended meaning and characterization of deconfined excitations and their statistics in mixed states are clarified. Moreover, when these deconfined anyons have nontrivial braiding statistics, we prove that the mixed states cannot be prepared via finite-depth local quantum channels from any bipartite separable states. We further demonstrate our construction using the decohered Kitaev honeycomb model and the decohered double semion model. In the latter case, a surprising scenario arises where decoherence gives rise to additional types of deconfined anyons.

I. INTRODUCTION

As long-range entangled (LRE) quantum matter, topologically ordered phases have attracted extensive attention in the past few decades [1–6]. Recently, there is a growing number of theoretical proposals [7–15] as well as experimental evidence [16–21] showing that topological order (TO) can be prepared in current many-body quantum simulation platforms, such as superconducting qubit arrays, Rydberg atom arrays, and trapped ion systems, etc. A key feature of these noisy intermediate-scale quantum (NISQ) devices is the inevitable presence of decoherence, which renders the quantum state a mixed state [22]. Substantial progress has been made in diagnosing nontrivial topological phases subject to decoherence [23–40]. Particularly, the decoherence-induced breakdown of topological quantum memory in the toric code model is investigated, and is related to the transition in the mixed-state topological order [31, 33]. The topological order therein is inherited from the pure-state counterpart, which is resistant to modest decoherence. Above certain critical error rate, the long-range entanglement is destroyed.

We are interested in the following question: Other than destroying the pure-state topological order, can decoherence give rise to novel types of quantum topological order that are intrinsically mixed? The possibility of such intriguing scenario arises from new mechanisms of anyon proliferation provided by decoherence, distinct from anyon condensation in pure states [41–43]. As a starting point, we explore such possibility in the context of \mathbb{Z}_2 (toric-code) topological order, which comprises

three types of anyon excitations, e, m , and $f = e \times m$, [44–51]. In pure states, either e or m (both being self-bosons) can condense, leading to a topologically trivial Higgs/confined phase [52]. Correspondingly, proliferation of e, m anyons induced by decoherence also destroys long-range entanglement. In contrast, f anyons are self-fermions, and therefore they cannot condense in pure state; instead, strong fluctuation of f anyons typically leads to a gapless spin liquid, which remains LRE. This motivates us to study the fate of \mathbb{Z}_2 topological order when f anyons proliferate under decoherence.

Specifically, we study the behavior of the toric code model [51] under local quantum channels that solely create f anyons. The topological quantum memory degrades to classical memory above certain decoherence threshold, aligning with previous studies. However, it turns out that the mixed state still possesses nontrivial quantum topological order even in the absence of quantum memory. To diagnose the mixed-state topological order, we employ the topological entanglement negativity (TEN) [53–56], which is a natural generalization of the topological entanglement entropy (TEE) [57, 58]. TEN has been utilized to probe topological order in thermal equilibrium [59–62] or under shallow-depth noise channels [31], effectively acting as a faithful indicator of topological quantum memory in those studied cases. However, we find that the TEN fails to reflect topological quantum memory in this scenario, and remains unchanged across the transition. Nevertheless, the nonzero TEN still points to the persistence of long-range entanglement, a hallmark of quantum topological order. Moreover, the absence of topological quantum memory indicates that the identified topological order has no pure-state counterpart and, therefore, is termed “intrinsic mixed-state quantum topological order” here.

We then provide further understanding of this peculiar result from the perspective of quantum anomalies.

* These authors contributed equally to this work.

† wangzhongemail@tsinghua.edu.cn

Crucially, the noisy channel proliferating f anyons preserves an anomalous 1-form symmetry generated by f anyons [63–65]. Through the anomalous 1-form symmetry, we show that the intrinsic mixed-state quantum TO in the decohered toric code supports deconfined fermionic anyons, with a detailed explanation of the extended meaning of deconfinement and fermionic statistics in mixed states. We generally prove that mixed states with anomalous 1-form symmetries must be LRE. Moreover, we show that when the anomalous 1-form symmetry is generated by anyons with nontrivial braiding statistics, any two complementary parts of the mixed state are LRE (for arbitrary bipartition), generalizing the conjecture “mixed-state anomaly \Rightarrow multipartite non-separability” in [66], which focuses on 0-form symmetries. With this perspective, our construction can be straightforwardly generalized to get other intrinsic mixed-state quantum TO, characterized by deconfined anyons with nontrivial statistics. We give two more examples, the decohered Kitaev honeycomb model and the decohered double semion model. In the latter example, we find more surprising features in mixed-state TO. In addition to peeling off anyons in the original TO, decoherence can even give birth to new types of deconfined anyons, which leads to a non-modular anyon theory in our case.

The rest of the paper is organized as follows. In Section II we construct an intrinsic mixed-state quantum TO by proliferating f anyons in the toric code, and reveal its properties through investigations of information quantities including the coherent information and the TEN. We also discuss similarities and disparities to the gapless spin liquid phase in pure states. In Section III we discuss general aspects of intrinsic mixed-state from the perspective of 1-form symmetry anomalies and deconfined excitations. In Section IV we generalize our construction of mixed-state quantum TO to decohered Kitaev honeycomb model and decohered double semion model. We conclude with a discussion in Section V.

II. DECOHERED TORIC CODE AS INTRINSIC MIXED-STATE QUANTUM TO

A. The model

We start with the 2D \mathbb{Z}_2 toric code model on a square lattice:

$$H_{\text{TC}} = -\sum_v A_v - \sum_p B_p, \quad A_v \equiv \prod_{i \in v} X_i, \quad B_p \equiv \prod_{i \in p} Z_i,$$

where X_i, Z_i are Pauli matrices. The ground states are 4-fold degenerate and can be used to encode two logical qubits, amenable to fault-tolerant quantum information processing. The tolerance of the topological quantum memory against local phase errors and bit flip errors has been investigated in [23, 31, 33], where errors are modeled

as local quantum channels, \mathcal{N}^z and \mathcal{N}^x ,

$$\begin{aligned} \mathcal{N}^x &= \prod_i \mathcal{N}_i^x, \mathcal{N}_i^x[\cdot] \equiv (1 - p_x) \cdot + p_x X_i \cdot X_i, \\ \mathcal{N}^z &= \prod_i \mathcal{N}_i^z, \mathcal{N}_i^z[\cdot] \equiv (1 - p_z) \cdot + p_z Z_i \cdot Z_i. \end{aligned} \quad (1)$$

p_x, p_z are the error rates of bit flip and phase errors respectively. Since these channels incoherently create e, m anyons, respectively, we denote the corresponding error-corrupted states as ρ_e, ρ_m . It has been shown that above the error threshold, the proliferation of either bosonic anyon (e or m) would degrade the quantum memory to classical memory, accompanied by a sudden drop of TEN from $\log 2$ to 0. This motivates us to investigate the incoherent proliferation of the fermionic f anyons of the \mathbb{Z}_2 topological order, which can be realized by the following 2-qubit quantum channel:

$$\mathcal{N}^f = \prod_i \mathcal{N}_i^f, \mathcal{N}_i^f[\cdot] := (1 - p_f) \cdot + p_f Z_i X_{i+\delta} \cdot X_{i+\delta} Z_i, \quad (2)$$

where $\delta = (\frac{1}{2}, -\frac{1}{2})$ (the lattice constant is taken to be 1) and $0 < p_f < \frac{1}{2}$ is the error rate. In this way the ground state ρ_0 is turned into a mixed state, $\rho_f = \mathcal{N}^f[\rho_0]$. As depicted in Fig. 1(b), \mathcal{N}^f exclusively creates f anyons. In contrast, certain other types of errors, like the Pauli-Y errors, locally create pairs of f anyons as well, but globally they also produce e and m anyons, resulting in completely different outcomes. In the following sections, we demonstrate that this simple model surprisingly realizes an exotic intrinsic mixed-state quantum topological order through analytical exact investigations of its topological memory and topological entanglement negativity.

B. Breakdown of quantum memory

Under the \mathcal{N}^f channel, the mixed state undergoes an error-induced transition corresponding to the breakdown of quantum memory, similar to the case with bit flip and phase errors. Such transitions can be probed by information quantities nonlinear in the density matrix, such as the coherent information $I_c = S(\rho_f) - S(\rho_{Rf})$ [31, 67, 68], where S is the von Neumann entropy. R denotes reference qubits purifying the initial state ρ_0 , which is taken to be the maximally mixed state in the code space,

$$\rho_0 = \frac{1}{4} \prod_v \frac{1 + A_v}{2} \prod_p \frac{1 + B_p}{2} = \text{tr}_R(|\Psi\rangle\langle\Psi|), \quad (3)$$

and $\rho_{Rf} = \mathcal{I}_R \otimes \mathcal{N}^f[|\Psi\rangle\langle\Psi|]$ is the decohered density matrix. The coherent information measures the amount of information transmitted by the noisy channel \mathcal{N} , or in other words, it diagnoses the ability to restore the information encoded in the code space via error correction. Due to the subadditivity of the von Neumann entropy, the coherent information is bounded by $-S(\rho_0) \leq$

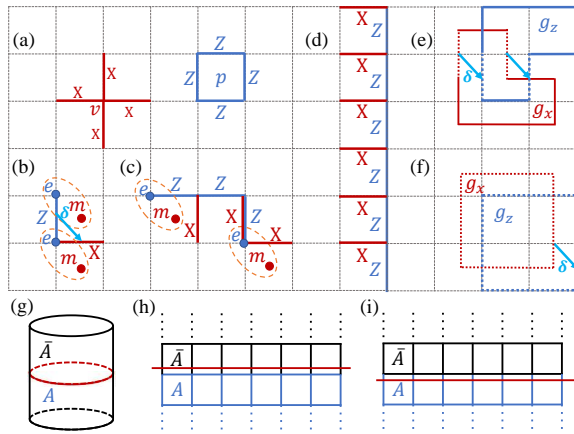


FIG. 1. (a). A_v and B_p . (b). The Kraus operator $Z_i X_{i+\delta}$ of the quantum channel \mathcal{N}_i^f creates a pair of f anyons, labeled by orange ellipses. (c). An example of an error string C (the blue line) and $W_C^f = \prod_{i \in C} Z_i X_{i+\delta}$. f anyons are created at the ends of C . (d). A non-contractible loop operator $W_{\tilde{\gamma}_y}$ along y direction. (e). A typical loop configuration $g = g_x g_z$, with g_x colored in red and g_z in blue. The dashed/solid lines represent segments where g_x, g_z coincide/do not coincide (up to a shift by δ). $l_g = 12$ in this example. (f). An example of a tensionless loop configuration, i.e., $l_g = 0$. (g). Bipartition of a cylinder. (h)-(i) Two ways of bipartitions.

$I_c \leq S(\rho_0)$, and the sufficient and necessary condition for the existence of perfect quantum error correction is that $I_c = S(\rho_0)$ [67]. The error threshold p_c corresponding to a sudden drop of I_c captures the breakdown of quantum memory, and this error rate threshold is an intrinsic threshold, which means for error rate $p > p_c$ there is no decoding algorithm to recover the encoded quantum information.

In our model, we find that I_c can be exactly mapped to the free energy cost of non-contractible defect lines of the random bond Ising model (RBIM) along the Nishimori line [69], using the replica trick:

$$\begin{aligned}
 I_c &= -\lim_{n \rightarrow 1} \frac{\partial}{\partial n} \text{Tr}(\rho_f^n) + \lim_{n \rightarrow 1} \frac{\partial}{\partial n} \text{Tr}(\rho_{Rf}^n) \\
 &= 2 \log 2 - \log \frac{\sum_{d_x, d_y=0,1} Z_{d_x, d_y}^{\text{RBIM}}}{Z_{00}^{\text{RBIM}}} \\
 &= 2 \log 2 - \log \left[\sum_{d_x, d_y=0,1} e^{-\Delta F_{d_x, d_y}} \right],
 \end{aligned} \tag{4}$$

where $\Delta F_{d_x, d_y}$ is the excess free energy with the insertion of a non-contractible defect line, and d_x, d_y count the number of non-contractible defect lines in the x and y directions, respectively. The derivation of the above mapping of I_c can be found in Appendix A 1.

For small p , the RBIM is in the ferromagnetic (FM) phase, and the excess free energy of a defect line is extensive, $\Delta F_{\{d_x, d_y\} \neq \{0,0\}} \sim O(L)$, which leads to $I_c = 2 \log 2$. At a critical error rate $p_c \approx 0.109$, the RBIM undergoes

a ferromagnet-to-paramagnet phase transition, with an abrupt drop of coherent information, which determines the threshold where the topological quantum memory is damaged beyond recovery. Nevertheless, we note that ρ_f still retains classical memory for $p_f > p_c$. Suppose the initial state ρ_0 is in an eigenspace of the logical operators $W_{\tilde{\gamma}_{x,y}} = \prod_{i \in \tilde{\gamma}_{x,y}} X_i Z_{i+\delta}$, where $\tilde{\gamma}_x, \tilde{\gamma}_y$ are two non-contractible loops on the dual lattice. Then ρ_f always stays in the same eigenspace under the quantum channel, as $[W_{\tilde{\gamma}_{x,y}}, Z_i X_{i+\delta}] = 0$.

C. Topological entanglement negativity

Based on the above analysis, it may seem that ρ_f closely resembles ρ_e and ρ_m . However, surprisingly, we demonstrate below that even when the quantum memory breaks down for $p_f > p_c$, ρ_f retains LRE with a nonzero TEN, indicating the emergence of a distinct quantum topological order.

To evaluate the entanglement negativity of ρ_f and its scaling, we take the cylinder geometry with the bipartition $A \cup \bar{A}$ as depicted in Fig. 1(g). Then the logarithmic negativity is defined as:

$$\varepsilon_A(\rho_f) \equiv \log \|\rho_f^{T_A}\|_1 = \varepsilon_{\bar{A}}(\rho_f), \tag{5}$$

where T_A denotes the partial transpose of ρ_f in subregion A , and $\|\cdot\|_1$ represents the trace norm. As an entanglement monotone, the logarithmic negativity is commonly used to quantify quantum entanglement in mixed states, excluding the contribution from classical correlation [70–73]. As such, it is considered a natural generalization of entanglement entropy in pure states.

For convenience, we take the initial state ρ_0 to be the maximally mixed state in the code space (3). We denote the groups generated by $\{A_v\}, \{B_p\}$ as $G_{x(z)}$:

$$G_x \equiv \{\{A_v\}\}, G_z \equiv \{\{B_p\}\}. \tag{6}$$

Each group element $g_{x(z)}$ corresponds to a loop configuration on the dual lattice (original lattice), as shown in Fig. 1(e), (f). Thus, ρ_0 can be represented by an equal weight expansion of loop configurations:

$$\rho_0 = \frac{1}{2^N} \sum_{g_x \in G_x} \sum_{g_z \in G_z} g_x g_z = \frac{1}{2^N} \sum_{g \in G \equiv G_x \times G_z} g. \tag{7}$$

The effect of \mathcal{N}^f is to introduce loop tension. Specifically, for a given loop $g = g_x g_z$, \mathcal{N}^f assigns a weight $1 - 2p_f$ to each segment where g_x and g_z does not coincide (up to a shift by δ). Consequently, we have,

$$\rho_f = \mathcal{N}^f[\rho_0] = \frac{1}{2^N} \sum_{g \in G} (1 - 2p_f)^{l_g} g, \tag{8}$$

where l_g is the length of segments where g_x and g_z do not coincide. In Fig. 1(e) we illustrate how to count such segments, and in Fig. 1(f) we give an example of a tensionless loop.

Now we take the partial transpose for subregion A . We denote $g = g_{A\bar{A}}$, where $g_{A(\bar{A})}$ is the restriction of operator g to subregion $A(\bar{A})$,

$$\rho_f^{TA} = \frac{1}{2^N} \sum_{g \in G} (1 - 2p_f)^{l_g} y_A(g) g, \quad (9)$$

and $y_A(g) = 1(-1)$ when g_{xA} and g_{zA} commute (anti-commute).

As shown in Fig. 1(g)-(i) there are two possible choices of translation-invariant entanglement cut, which lead to slightly different results on TEN. Remarkably, for the bipartition in Fig. 1(h), the final result of negativity is rather simple, and is independent of p_f :

$$\varepsilon_A(\rho_f) = L \log 2 - \log 2, \quad (10)$$

where L is the length of the boundary between A and \bar{A} . For the bipartition in Fig. 1(i), however, the calculation of negativity is much harder for general p_f . Here we only show the results for the case with maximal decoherence, $p_f = \frac{1}{2}$, which is expected to reflect general features of the mixed states for $p_f > p_c$. In this case ρ_f becomes the maximally mixed state with $W_p \equiv A_{p-\delta} B_p = 1, \forall p$.

$$\rho_f = \frac{1}{2^{N/2+1}} \prod_p \frac{1 + W_p}{2} \quad (11)$$

It turns out the negativity exhibits an unusual dependence on the parity of L :

$$\varepsilon_A(\rho_f) = \begin{cases} \frac{L}{2} \log 2 - \log 2, & \text{if } L \text{ is even,} \\ \frac{L}{2} \log 2 - \frac{\log 2}{2}, & \text{if } L \text{ is odd.} \end{cases} \quad (12)$$

In all the above results, the entanglement negativity satisfies an area law, and has an $O(1)$ subleading term, known as the topological entanglement negativity, which is a generalization of TEE. A nonzero value of TEN signals nontrivial quantum TO, as it arises solely from long-range entanglement. For example, $\text{TEN} = \log 2$ for the toric-code ground state. Hence, it has been used to diagnose topological order in both finite-temperature systems [60] and states subject to local errors [31]. Notably, in our model, the TEN remains nonzero even if quantum memory is gone, which is in sharp contrast to the case with single-qubit X or Z errors.

The dependence of TEN on the boundary size for the second type of bipartition seems a bit puzzling. However, for pure-state topological order, similar behavior of the even/odd dependence on system size also exist. Namely, for \mathbb{Z}_2 topological order enriched by translation symmetry through weak symmetry breaking, typical examples include the Wen-plaquette model and the Abelian phase of Kitaev honeycomb model [74, 75]. In these cases, it is well known that the ground state degeneracy on a torus also exhibits similar dependence on the system size. Although there is little discussion in literature about how

weak symmetry breaking affects entanglement properties, it is straightforward to check that the subleading term of bipartite entanglement entropy on a cylinder also depends on the parity of the boundary size in these models. Based on this observation, we establish a connection between the entanglement properties of ρ_f and ground-state \mathbb{Z}_2 topological order enriched by translation symmetry in Appendix A 4.

We emphasize that the persistence of long-range entanglement signifies genuine quantum TO, which distinguishes ρ_f from the so-called classical TO, a concept raised in the study of finite-temperature TO [60, 76–78]. States with classical TO have topological classical memory as well, but zero TEN. One typical example is the low-temperature phase of the 3D toric code model. In this sense, ρ_e and ρ_m (above the error threshold) also have classical TO. ρ_f is qualitatively different from these known examples.

D. Robustness of the intrinsic mixed-state quantum TO

Although in our construction we need to use specific 2-qubit channels that looks a bit unconventional, ρ_f represents a new type of topologically ordered phase, instead of a fine-tuned exception. We can consider the case when single-qubit phase errors are also present: $\rho_{f,e} = \mathcal{N}^z[\rho_f]$, with error rate p_z . By mapping to two decoupled RBIMs (see Appendix A 5 for details), we demonstrate that for small p_z , $\rho_{f,e}$ stays in the same phase as ρ_f , while for $p_z > p_c \approx 0.109$, the state undergoes another transition to the trivial phase, with no memory and zero TEN.

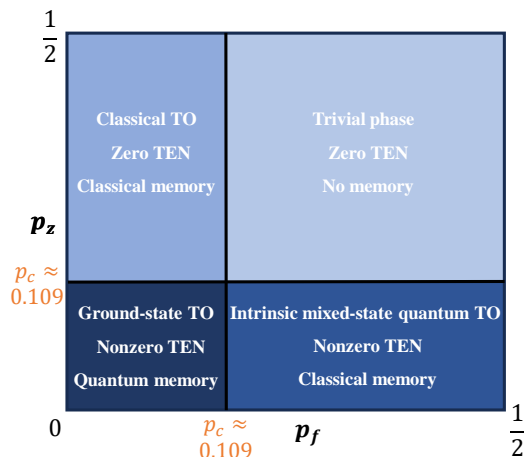


FIG. 2. The phase diagram of the toric code model subject to both two-qubit errors and single-qubit phase errors. Properties of each phase, including topological memory, TEN, and superselection sectors are indicated in the phase diagram.

E. Comparison to anyon condensation and gapless spin liquid

From the previous analysis, we see that although ρ_f only exhibits classical memory (for $p_f > p_c$), it is fundamentally distinct from ρ_e and ρ_m . To gain deeper insight into this counter-intuitive result, we draw comparisons between the error-induced anyon proliferation and anyon condensation in pure states. Instead of applying local quantum channels, we analyze the case when the $X_i, Z_i, Z_i X_{i+\delta}$ terms are directly introduced into the toric code Hamiltonian:

$$H = H_{\text{TC}} - \sum_i h_x X_i - h_z Z_i - h_{xz} Z_i X_{i+\delta}, \quad (13)$$

The ground state phase diagram for $h_{xz} = 0$ has been extensively studied [52, 79–82]. For sufficiently large h_z or h_x , it leads to the condensation of e or m anyons, respectively, resulting in the destruction of long-range entanglement. Analogously, the local Z, X errors induce e, m anyon proliferation in an incoherent manner, which also destroys the long-range entanglement. Despite the similarities between decoherence-induced anyon proliferation and anyon condensation, there are still noteworthy distinctions. In mixed states, incoherent proliferation of either e or m does not completely trivialize the phase but rather leads to classical TO. Contrarily, in pure states, condensation of either e or m already leads to the trivial Higgs/confined phase.

The distinction becomes much more significant for f anyons. As fermions, they cannot condense in pure states. Then what happens when we turn on fluctuations of f anyons ($h_{zx} \neq 0$)? Surprisingly, at $h_z = h_x = 0$, this model can be exactly solved via fermionization [83]. As we show in Appendix B, when h_{xz} is sufficiently large ($h_{x,z} = 0$), corresponding to large fluctuations of f particles, the system enters a gapless spin liquid phase, where f particles form a p -wave superconductor with conic dispersion, similar to the gapless Kitaev spin liquid [75]. The intrinsic mixed-state quantum TO proposed in this paper has many common features with the gapless spin liquid. First, they are both obtained by proliferating f anyons in the \mathbb{Z}_2 TO, and, as a result, they both have no quantum memory. For the gapless spin liquid, it is due to the absence of a spectrum gap, so there is no well-defined topological degeneracy. Second, despite the lack of quantum memory, they are both LRE, and are thus nontrivial phases of matter. In the next section we will uncover a deeper reason of their LRE nature from the perspective of anomalies. However, there are also notable differences between ρ_f and the gapless spin liquid phase. Gapless phases typically exhibit critical behaviors, including algebraically decaying correlation functions and subleading logarithmic corner contributions to entanglement entropy/negativity [84–86]. Contrarily, since ρ_f is obtained by applying local quantum channels on a gapped topological order, no power-law correlation can be generated, i.e., ρ_f exhibits short-range correlation for all local op-

erators, which is a prerequisite for any topological order. Moreover, as we have seen, the subleading term in the entanglement negativity $\varepsilon_A(\rho_f)$ is always $O(1)$ for ρ_f . In this sense, ρ_f also retains certain essential properties of gapped topological order. Therefore, ρ_f indeed represents a new type of topological order that is only possible in mixed states. The similarities and differences between gapless spin liquid and intrinsic mixed-state quantum TO are summarized in Table I.

	Gapless spin liquid	Intrinsic mixed-state quantum TO
Quantum memory	×	×
Long-range entanglement	✓	✓
Correlation of local operators	Power-law correlation	Short-range correlation
Anomalous 1-form symmetry	✓	✓
Deconfined fermions	✓	✓

TABLE I. Comparison between the gapless spin liquid and the intrinsic mixed-state quantum TO (ρ_f). See Section III for properties listed in the last two rows

III. GENERALITIES: ANOMALOUS 1-FORM SYMMETRY, NONTRIVIAL STATISTICS, AND LONG-RANGE ENTANGLEMENT

The long-range entanglement of the gapless spin liquid and the intrinsic mixed-state quantum TO are both related to an anomalous 1-form symmetry, which is generated by the following loop operators

$$W_{\tilde{\gamma}}^f = \prod_{i \in \tilde{\gamma}} X_i Z_{i+\delta}, \quad (14)$$

where $\tilde{\gamma}$ denotes an arbitrary loop on the dual lattice [63, 64]. For non-contractible loops $\tilde{\gamma} = \tilde{\gamma}_{x,y}$, $W_{\tilde{\gamma}}^f$ are the logical operators responsible for the classical memory of ρ_f (see 1(d)). These loop operators generate a symmetry of both models because $[W_{\tilde{\gamma}}^f, H_{\text{TC}}] = [W_{\tilde{\gamma}}^f, Z_i X_{i+\delta}] = 0$. Particularly, we have $W_{\tilde{\gamma}}^f \rho_f = \rho_f$ [87], which is known as the strong symmetry condition for the mixed state [28, 34, 88, 89]. For an open string \tilde{C} , $W_{\tilde{C}}^f = \prod_{i \in \tilde{C}} X_i Z_{i+\delta}$ creates two f anyons at the ends of the string, so they are referred to as f strings, and the 1-form symmetry is said to be generated by f anyons. The nontrivial statistics of f anyons indicates an anomaly of the 1-form symmetry [64]. We show below that, as a consequence of the anomalous strong 1-form symmetry, the mixed state ρ_f still has deconfined fermionic excitations.

The above statement might be confusing at first sight. Since the f anyons already proliferate in ρ_f , what are

the deconfined fermions then? Perhaps the easiest way to resolve this apparent paradox is to vectorize ρ in the double Hilbert space: $\rho = \sum_{mn} \rho_{mn} |m\rangle\langle n| \rightarrow |\rho\rangle\rangle = \sum_{mn} \rho_{mn} |m\rangle_+ \otimes |n\rangle_-$. For concreteness we choose the basis $\{|m\rangle\}$ as eigenstates of Z_i . Then $|\rho_0\rangle\rangle$ corresponds to two copies of toric-code ground states, with superselection sectors $\{1, e_+, m_+, f_+\} \times \{1, e_-, m_-, f_-\}$. The incoherent proliferation of f corresponds to condensation of $f_+ f_-$ in this picture, which leaves f_+ a deconfined excitation, though it should be now identified with f_- due to the condensation of $f_+ f_-$ [32]. Do these f_+ anyons correspond to physical excitation in the original Hilbert space? Although the naive way to create f_+ anyons $\rho_f \rightarrow W_{\tilde{C}}^f \rho$ is not a legitimate physical process, they can be created using the unitary process $\rho_f \rightarrow \rho'_f = U_{\tilde{C}} \rho_f U_{\tilde{C}}^\dagger$, with $U_{\tilde{C}} = \frac{I + iW_{\tilde{C}}^f}{\sqrt{2}}$. Then $f_{+/-}$ anyons appear in the interference terms. In this sense f anyons (we omit the “+” hereafter) remain physically meaningful excitations.

Now we address another subtle question: What does “deconfinement” really mean in mixed states under noisy channels? Conventionally, it means that the energy cost does not grow indefinitely by separating individual topological excitations far apart. Here this definition does not make sense because the system is no longer governed by a Hamiltonian. Therefore, we propose the following definition of deconfined excitations for generic mixed states.

Definition 1. Given a density matrix ρ , a pair of deconfined excitations are said to be created at locations i, j in the unitary process $\rho \rightarrow U \rho U^\dagger$, iff the following two conditions are satisfied:

1. The excitations cannot be created locally and individually. In other words, U cannot be any unitary operator supported near i, j . Typically, U is supported on an open string with endpoints i, j .
2. For any local operator O whose support is away from i, j , $\text{tr}(\rho O) = \text{tr}(U \rho U^\dagger O)$. It means that the change can only be detected near i, j .

Clearly, the above definition is consistent with the conventional notion of deconfined excitations, and serves as a faithful and natural generalization to open quantum systems. Next, we illustrate that f anyons (we omit the “+” hereafter) are indeed deconfined excitations according to this definition, created by the unitary operator $U_{\tilde{C}}$. The second condition can be easily verified using the strong 1-form symmetry. We denote the support of O as $\Omega(O)$ for convenience, which we assume to be away from i, j . If $\Omega(O) \cap \tilde{C} = \emptyset$, then $\text{tr}(U_{\tilde{C}} \rho U_{\tilde{C}}^\dagger O) = \text{tr}(\rho U_{\tilde{C}}^\dagger O U_{\tilde{C}}) = \text{tr}(\rho O)$; if $\Omega(O) \cap \tilde{C} \neq \emptyset$, we can always find another open string \tilde{C}' , such that $\tilde{C} \cup \tilde{C}'$ is a contractible loop and $\Omega(O) \cap \tilde{C}' = \emptyset$. Using the strong 1-form symmetry $U_{\tilde{C}'}^\dagger U_{\tilde{C}} \rho_f = \rho_f$, it is straightforward to get $\text{tr}(U_{\tilde{C}} \rho U_{\tilde{C}}^\dagger O) = \text{tr}(U_{\tilde{C}'} \rho U_{\tilde{C}'}^\dagger O) = \text{tr}(\rho O)$. The first condition follows from the fermionic statistics

of the f anyons [90]. See also the discussion below and in Section III.

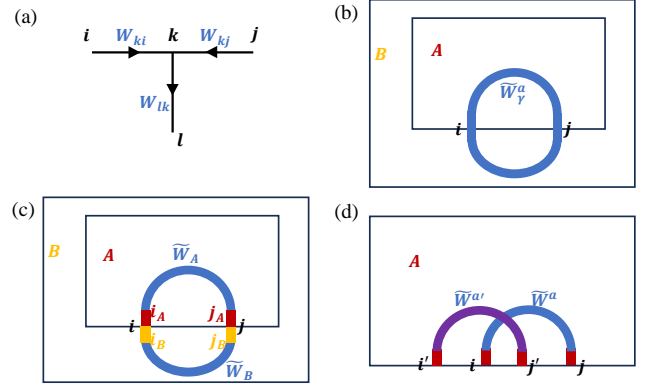


FIG. 3. (a). The exchange statistics of identical Abelian anyons can be defined using the open anyon strings W_{ki}, W_{kj}, W_{ik} . In defining open anyon strings, we require that two short strings can combine into a longer string: $W_{i_3 i_2} W_{i_2 i_1} = W_{i_3 i_1}$. (b). A closed a string that intersects ∂A at i, j . (c). Partition of W_γ^a into three parts: the open string $W_{i_A j_A}, W_{j_B i_B}$ supported completely on region A, B , and the middle red and orange segments W_{AB} straddling between A and B . (d). Anyon strings of a and a' .

Is the fermionic statistics well-defined for mixed states? We give an affirmative answer with the following microscopic method of detection (see Fig. 3 for an illustration): *a.* Create two f anyons at locations i, j using $W_{ji}^f = W_{jk}^f W_{ki}^f$; *b.* move the f anyon at i to location l using $W_{li}^f = W_{lk}^f W_{ki}^f$. *c.* move the other f anyon from j to i using $W_{ij}^f = W_{ji}^{f\dagger}$; *d.* move the f anyon at l to location j using $W_{jl}^f = W_{jk}^f W_{kl}^f$; *e.* annihilate the two f anyons using W_{ij}^f . In step *b-d* the locations of the two f anyons are exchanged, which result in a phase $W_{jl}^f W_{ij}^f W_{li}^f = \theta(f) = -1$. To turn this statistical phase into an observable effect, we can use the same protocol as in [17]. That is, we introduce an ancilla qubit and prepare the initial state $|+\rangle\langle+| \otimes \rho_f$, where $|+\rangle \equiv \frac{|1\rangle + |0\rangle}{\sqrt{2}}$. Then we can use the ancilla qubit to control the exchange process. Namely, we perform step *a-e* when the ancilla is in state $|1\rangle$, and do nothing otherwise. This controlled process can be performed using the unitary operator $V = \frac{1}{\sqrt{2}}(|0\rangle\langle 0| \otimes I + |1\rangle\langle 1| \otimes W_{ij}^f W_{jl}^f W_{ij}^f W_{li}^f W_{ji}^f)$. Then the statistical phase will manifest as the rotation of the ancilla:

$$V(|+\rangle\langle+| \otimes \rho_f) V^\dagger = |-\rangle\langle-| \otimes \rho_f, \quad (15)$$

where $|-\rangle = \frac{|0\rangle - |1\rangle}{\sqrt{2}}$. The fermionic statistics of emergent deconfined excitations is the most striking observable effect of the intrinsic mixed-state quantum TO. Here, it is guaranteed by the anomalous strong 1-form symmetry.

In the double space, $e_+ e_-$ also remains a deconfined excitation, which has mutual semion statistics with f_+ . Sur-

prisingly, this braiding statistics can also be (partially) detected in the physical Hilbert space, as we demonstrate below. First, note that ρ_f preserves a weak 1-form symmetry generated by e anyons, $W_\gamma^e \rho_f W_\gamma^e = \rho$ for contractible closed e string W_γ^e [28]. Then based on Definition 1, deconfined excitations can be created using an open e string, $\rho_f \rightarrow \rho_f^e = W_C^e \rho_f W_C^e$. Secondly, introduce an ancilla qubit and prepare the initial state $|+\rangle\langle+| \otimes \rho_f^e$. Then use the ancilla qubit to control the braiding process: if the ancilla is in $|1\rangle$, we create two f anyons and drag one of them along a loop l enclosing the e anyon, and finally annihilate with the other f anyon; if the ancilla is in $|0\rangle$ we do nothing. This controlled process can be performed using the unitary gate $V = \frac{1}{\sqrt{2}}(|0\rangle\langle 0| \otimes I + |1\rangle\langle 1| \otimes W_{\tilde{\gamma}}^f$, where $W_{\tilde{\gamma}}^f = \prod_{i \in \text{loop } \tilde{\gamma}} X_i Z_{i+\delta}$. Then the braiding statistics can be detected by rotation of the ancilla qubit:

$$V(|+\rangle\langle+| \otimes \rho_f^e) V^\dagger = |-\rangle\langle-| \otimes \rho_f^e. \quad (16)$$

Stated more formally, the braiding statistics reflects the mixed anomaly between the weak 1-form symmetry (generated by e) and the strong 1-form symmetry (generated by f) [91].

One key distinction to the usual anyon braiding is that the $f - e$ braiding here is only one-way defined. Namely, the statistical phase can only be detected by moving f around e (in a way that is controlled by the ancilla, as demonstrated above), but not the other way around. This directly follows from the fact that while f anyons generate a strong 1-form symmetry, e anyons only generate a weak 1-form symmetry. Therefore, a finer characterization of deconfined excitations than Definition 1 is needed, and we call the former type as strongly deconfined and the latter type as weakly deconfined. As demonstrated above, strongly deconfined anyons are allowed to form coherent superposition states, and their statistics can be detected from the interference effects. Weakly deconfined anyons, on the other hand, always have trivial exchange and braiding statistics among themselves and can have one-way braiding statistics with strongly deconfined anyons. In the rest of the paper we mainly focus on strongly deconfined anyons.

Using the perspective of anomalies, we can generalize our construction to obtain other intrinsic mixed-state quantum TO [92]. Given a TO with anyon content \mathcal{A} , one can incoherently proliferate a subset $\mathcal{B} \subset \mathcal{A}$ of anyons using a noisy channel, taking the Kraus operator to be the shortest string of anyons in \mathcal{B} . If there exists some Abelian anyon $a \in \mathcal{A}$ that have trivial braiding with all anyons in \mathcal{B} , then closed a strings commute with the Kraus operators. Therefore, the a anyons generate a strong 1-form symmetry. Based on the previous discussion, it means they remain deconfined excitations with well-defined statistics. When they have non-trivial statistics, $\theta(a) \neq 1$, then the 1-form symmetry is anomalous. For example, in the model discussed above, $\mathcal{A} = \{1, e, m, f\}$, $\mathcal{B} = \{f\}$, and $a = f$ because fermions have trivial full braiding with themselves.

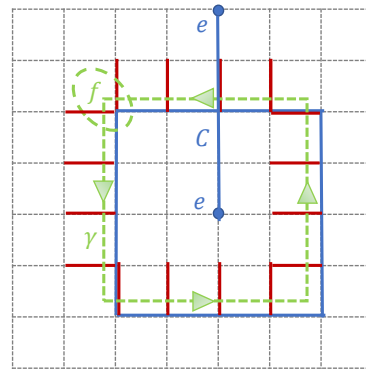


FIG. 4. Braiding between f and e . The quantum channel \mathcal{N}^f does not affect the braiding statistics because it preserves the weak 1-form symmetry generated by e and the strong 1-form symmetry generated by f .

The existence of non-bosonic strongly deconfined excitation can be viewed as another diagnosis of nontrivial mixed-state quantum TO, in complementary to TEN. Indeed, we show below that this property generically implies the mixed state to be LRE, without explicit calculation of negativity.

Theorem 1: Consider a 2-dimensional state ρ with anomalous strong 1-form symmetry generated by some Abelian anyon a with $\theta(a) \neq 1$, i.e., $W_\gamma^a \rho = \rho$, where W_γ^a 's are closed a strings supported on any contractible loop γ . Then ρ cannot be prepared using a finite-depth local channel (FDLC) from any fully separable state:

$$\rho \neq \mathcal{N}_{\text{FDLC}} \left[\sum_\lambda p_\lambda \bigotimes_{\text{site } i} |\psi_i^\lambda\rangle\langle\psi_i^\lambda| \right] \quad (p_\lambda > 0). \quad (17)$$

Before the proof, we give some remarks regarding the above theorem.

1. Following [93, 94], (17) can be viewed as the definition of LRE for generic mixed states. Thus the above theorem tells us anomalous strong 1-form symmetries must lead to nontrivial mixed-state quantum TO.
2. Typically, the 1-form symmetry includes generators supported on non-contractible loops. However, here we only require the symmetry condition for contractible ones, enabling a much wider range of applications. For example, for the construction of intrinsic mixed-state quantum TO discussed above, the pre-decoherence state can be taken to be any state in the ground state subspace. The above theorem can also be applied to topologically trivial spatial manifold like a 2-sphere.
3. Similar to the discussion above (15), the anomaly manifests as the algebra of open string operators:

$$\begin{aligned} W_{i_3 i_2}^a W_{i_2 i_1}^a &= W_{i_3 i_1}^a, \quad W_{i_1 i_2}^\dagger = W_{i_2 i_1}, \\ W_{k_j}^a W_{l_k}^a W_{k_m}^a &= \theta(a) W_{k_m}^a W_{l_k}^a W_{k_j}^a \end{aligned} \quad (18)$$

Essentially, the nontrivial statistics $\theta(a) \neq 1$ of a is all we need in the following proof.

4. Notably, the condition we impose automatically includes the case of mixed anomaly between strong 1-form symmetries, which arises when two strongly deconfined Abelian anyons a, a' have nontrivial mutual statistics, $B_\theta(a, a') \neq 1$ ($B_\theta(a, a')$ is the statistical phase from a full braiding between a and a'). Using the relation $B_\theta(a, a') = \frac{\theta(aa')}{\theta(a)\theta(a')}$, the mixed anomaly implies at least one of a, a', aa' has nontrivial self statistics $\theta \neq 1$. Thus we do not need to consider mutual statistics separately.
5. To prove the theorem, we make an additional assumption that W_γ^a can be expressed using a FDLUC, which is usually the case for Abelian anyon a .

Proof. Suppose by contradiction that $\rho = \mathcal{N}_{\text{FDLC}}[\sum_\lambda p_\lambda \otimes_{\text{site } i} |\psi_i^\lambda\rangle\langle\psi_i^\lambda|]$. Recall that a generic FDLUC \mathcal{N} can be constructed in three steps: First, introduce auxiliary degrees of freedom on each site. Secondly, apply a finite-depth local unitary circuit (FDLUC) on the system and the auxiliary degrees of freedom. Finally, trace out the added degrees of freedom. It can be written as $\mathcal{N}_{\text{FDLC}}[\rho_0] = \text{tr}_E[U_{SE}\rho_0 \otimes_{\text{site } i} |e_i\rangle\langle e_i|U_{SE}^\dagger]$, where U_{SE} is a FDLUC. If ρ_0 is a fully separable state, then $\rho = \mathcal{N}_{\text{FDLC}}[\rho_0]$ is of the form $\rho = \sum_\lambda p_\lambda \text{tr}_E[U_{SE}|\phi_i^\lambda\rangle\langle\phi_i^\lambda|U_{SE}^\dagger]$, where $|\phi_i\rangle \equiv |\psi_i^\lambda\rangle \otimes |e_i^\lambda\rangle$. Then each pure state $U_{SE} \otimes_i |\phi_i\rangle$ must be symmetric: $W_\gamma^a U_{SE} \otimes_i |\phi_i\rangle = U_{SE} \otimes_i |\phi_i\rangle$. Equivalently, $\tilde{W}_\gamma^a = U_{SE}^\dagger W_\gamma^a U_{SE}$ is a symmetry of the product state $\otimes_i |\phi_i\rangle$. Crucially, the restriction of \tilde{W}^a to open strings $\tilde{W}_{i_1 i_2}^a \equiv U_{SE}^\dagger W_{i_1 i_2}^a U_{SE}$ satisfies the same algebra (18) as W^a . As we show below, this will lead to contradiction.

Since any contractible loop operator \tilde{W}_γ^a is a symmetry, an open string $\tilde{W}_{i_1 i_2}^a$ can only change the state near the end of the string: $\tilde{W}_{i_1 i_2}^a \otimes_i |\phi_i\rangle = A_{i_1} B_{i_2} \otimes_i |\phi_i\rangle$, where A_{i_1}, B_{i_2} are unitary operators supported near i_1, i_2 , respectively. From the algebraic relation (18),

$$\tilde{W}_{kj}^a \tilde{W}_{lm}^a = \theta(a) \tilde{W}_{km}^a \tilde{W}_{lj}^a. \quad (19)$$

By applying both sides of the equation on $\otimes_i |\tilde{\psi}_i\rangle$, we get $A_k \otimes B_j \otimes A_l \otimes B_m \otimes_i |\phi_i\rangle = \theta(a) A_k \otimes B_m \otimes A_l \otimes B_j \otimes_i |\phi_j\rangle$, which leads to contradiction when $\theta(a) \neq 1$. \square

The above proof shows that nontrivial quantum TO is guaranteed by the existence of non-bosonic deconfined excitation a , even for mixed states. Furthermore, when a is neither bosonic or fermionic, $\theta(a) \neq \pm 1$, or when a has nontrivial mutual statistics with another strongly deconfined anyon a' , then an even stronger conclusion can be proved.

Theorem 2: Consider a 2-dimensional state ρ with an anomalous strong 1-form symmetry generated by Abelian anyons a, a' with nontrivial braiding statistics,

$B_\theta(a, a') \neq 1$. Then for any bipartition $A \cup B$ with linear size $L_A, L_B \rightarrow \infty$ in the thermodynamic limit, ρ cannot be prepared using a FDLUC from any bipartite separable state:

$$\rho \neq \mathcal{N}_{\text{FDLC}}[\sum_\lambda p_\lambda |\psi_A^\lambda\rangle\langle\psi_A^\lambda| \otimes |\psi_B^\lambda\rangle\langle\psi_B^\lambda|]. \quad (20)$$

Again, we only need the symmetry condition $W_\gamma^a \rho = \rho, W_\gamma^{a'} \rho = \rho$ for contractible loops operators $W_\gamma^a, W_\gamma^{a'}$, which we assume to be FDLUC's.

Proof. Suppose, by contradiction, that $\rho = \mathcal{N}_{\text{FDLC}}[\sum_\lambda p_\lambda |\psi_A^\lambda\rangle\langle\psi_A^\lambda| \otimes |\psi_B^\lambda\rangle\langle\psi_B^\lambda|]$. Following the same steps as in the proof of Theorem 1, we have

$$\tilde{W}_\gamma^a |\phi_A\rangle \otimes |\phi_B\rangle = |\phi_A\rangle \otimes |\phi_B\rangle, \quad (21)$$

with the bipartite product state $|\phi_A\rangle \otimes |\phi_B\rangle$ and the 1-form symmetry generator \tilde{W}_γ^a defined in an enlarged Hilbert space $\mathcal{H}_S \otimes \mathcal{H}_E$. Next, we take a loop γ intersecting the boundary between A and B at locations i, j , with the corresponding closed a string \tilde{W}_γ^a . We extract a small segment of \tilde{W}_γ^a near the intersection points, denoted by \tilde{W}_{AB}^a , such that \tilde{W}_γ^a can be written as $\tilde{W}_\gamma^a = \tilde{W}_{i_A j_A}^a \tilde{W}_{j_B i_B}^a \tilde{W}_{AB}^a$, where $\tilde{W}_{i_A j_A}^a, \tilde{W}_{j_B i_B}^a$ are open a strings completely supported on A, B , respectively. Then we have

$$\begin{aligned} \tilde{W}_{AB}^a |\phi_A\rangle \otimes |\phi_B\rangle &= \tilde{W}_{i_A j_A}^{a\dagger} |\phi_A\rangle \otimes \tilde{W}_{j_B i_B}^{a\dagger} |\phi_B\rangle \\ &\Rightarrow \text{tr}_{B \cup \sigma_{ij}} [|\phi_A\rangle\langle\phi_A| \otimes |\phi_B\rangle\langle\phi_B|] \\ &= \text{tr}_{B \cup \sigma_{ij}} [\tilde{W}_{i_A j_A}^{a\dagger} |\phi_A\rangle\langle\phi_A| \tilde{W}_{i_A j_A}^a \otimes |\phi_B\rangle\langle\phi_B|] \\ &\Rightarrow \text{tr}_{\sigma_{ij}} [|\phi_A\rangle\langle\phi_A|] = \text{tr}_{\sigma_{ij}} [\tilde{W}_{i_A j_A}^{a\dagger} |\phi_A\rangle\langle\phi_A| \tilde{W}_{i_A j_A}^a], \end{aligned} \quad (22)$$

where σ_{ij} denotes the union of the two red segments in Fig.3(c). Due to the unitary equivalence of purification [95],

$$\begin{aligned} \exists u_{\sigma_{ij}} \text{ supported on } \sigma_{ij}, \text{ s.t. } u_{\sigma_{ij}} |\phi_A\rangle &= \tilde{W}_{i_A j_A}^{a\dagger} |\phi_A\rangle \\ \Rightarrow u_{\sigma_{ij}}^\dagger \tilde{W}_{j_A i_A}^a |\phi_A\rangle &= |\phi_A\rangle \end{aligned} \quad (23)$$

Physically, this means a pair of a and its antiparticle are created in the bulk of A , moving apart towards ∂A , and get eliminated on the boundary (by a unitary process with local support). Below we show such process contradicts with the anyonic statistics of a [96, 97]. Now consider the closed a' string $W_{\gamma'}^{a'}$ which intersects the boundary ∂A at i', j' , with the distance between i, j, i', j' sufficiently large compared to the depth of $\mathcal{N}_{\text{FDLC}}$. Similarly to the above analysis,

$$\exists u_{\sigma_{i'j'}} \text{ supported on } \sigma_{i'j'}, \text{ s.t. } u_{\sigma_{i'j'}}^\dagger \tilde{W}_{j'_A i'_A}^a |\phi_A\rangle = |\phi_A\rangle. \quad (24)$$

On the other hand, from the braiding statistics between a, a' :

$$\begin{aligned} \tilde{W}_{j'_A i'_A}^a \tilde{W}_{j_A i_A}^a &= B_\theta(a, a') \tilde{W}_{j_A i_A}^a \tilde{W}_{j'_A i'_A}^a \\ \Rightarrow u_{\sigma_{i'j'}}^\dagger \tilde{W}_{j'_A i'_A}^a u_{\sigma_{ij}}^\dagger \tilde{W}_{j_A i_A}^a &= B_\theta(a, a') u_{\sigma_{ij}}^\dagger \tilde{W}_{j_A i_A}^a u_{\sigma_{i'j'}}^\dagger \tilde{W}_{j'_A i'_A}^a, \end{aligned} \quad (25)$$

which is inconsistent with (23), (24) when $B_\theta(a, a') \neq 1$. \square

We can restate Theorem 2 in the following way: if a mixed state has strongly deconfined Abelian anyons with nontrivial braiding statistics, then for any bipartition, there must be long-range entanglement between the two complementary regions. Notably, our discussion includes the scenario $a' = a$, in which case $B_\theta(a, a') = \theta^2(a)$. Compared to Theorem 1, we leave behind the case that a has fermionic self-statistics but trivial mutual braiding statistics with other deconfined anyons. In such cases, a also generates an anomalous strong 1-form symmetry, but our proof does not work. Nevertheless, the decohered toric code under “ZX” errors we construct is indeed bipartite LRE, indicated by the nonzero TEN, which arguably should also be related to the anomalous strong 1-form symmetry generated by f anyons. It is intriguing to explore whether the existence of deconfined fermions also generically lead to bipartite LRE mixed states.

The above results can be viewed as a generalization of the results in [66], where it is conjectured that mixed states with anomalous strong 0-form symmetry in d spatial dimensions cannot be prepared via a FDLIC from any $(d+2)$ -partite separable states. In two dimensions it means the mixed states cannot be prepared via a FDLIC from a 4-partite non-separable state, with the additional condition that three of the four parts intersect at one point. Our results show that anomalies of 1-form symmetries can have a stronger constraining power, since bipartite non-separability implies multipartite non-separability, but not vice versa.

IV. GENERALIZATIONS TO OTHER INTRINSIC MIXED-STATE QUANTUM TO

A. Decohered Kitaev honeycomb model

In last section we provide a general route to generalize the construction in Section II to obtain other intrinsic mixed-state quantum TO. In this section we give two more examples as applications. We first discuss the generalization to the Kitaev honeycomb model: $H = -J_x \sum_{x\text{-bonds}} \sigma_j^x \sigma_k^x - J_y \sum_{y\text{-bonds}} \sigma_j^y \sigma_k^y - J_z \sum_{z\text{-bonds}} \sigma_j^z \sigma_k^z - \sum_i \vec{h} \cdot \vec{\sigma}_i$ (with $|\vec{h}| \ll |J_\mu|$, $\mu = x, y, z$). This model can be exactly solved by mapping it to Majorana fermions coupled to static \mathbb{Z}_2 gauge fields [51]. It is shown that the ground state ρ_0 of this model can realize Abelian \mathbb{Z}_2 TO, non-Abelian Ising TO, as well as a gapless \mathbb{Z}_2 spin liquid phase. All the three phases have deconfined fermion excitations.

To obtain intrinsic mixed-state quantum TO, we construct the following channel:

$$\rho_f = \mathcal{N}^X \circ \mathcal{N}^Y \circ \mathcal{N}^Z[\rho_0], \quad \mathcal{N}^\alpha = \prod_{(ij) \in \alpha\text{-bonds}} \mathcal{N}_{(ij)}^\alpha, \quad (26)$$

$$\mathcal{N}_{(ij)}^\alpha[\rho_0] = p \sigma_i^\alpha \sigma_j^\alpha \rho_0 \sigma_j^\alpha \sigma_i^\alpha + (1-p) \rho_0.$$

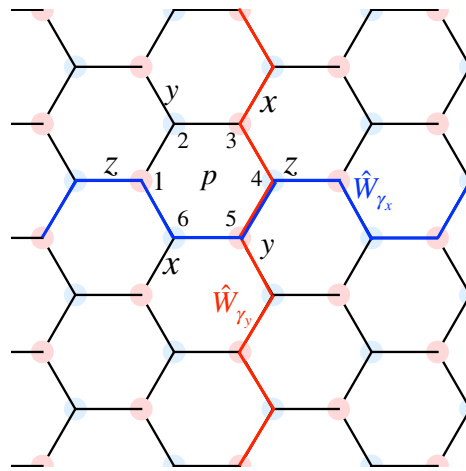


FIG. 5. The Kitaev honeycomb model, logical operators and flux operators. All the bonds are classified into three different equivalence classes of parallel bonds: x-bonds, y-bonds and z-bonds. There is a two-spin interaction $\sigma_i^\alpha \sigma_j^\alpha$ on each α -bond, where $\alpha = x, y, z$. The two non-contractible loop operators $W_{\gamma_x}, W_{\gamma_y}$ illustrated as blue and red are the product of the two-spin interactions on the bonds along those loops. In each plaquette p , there is a conserved flux operator $W_p^f = \sigma_1^z \sigma_2^y \sigma_3^x \sigma_4^z \sigma_5^y \sigma_6^x$.

This channel leads to decoherence of the fermions but preserves the \mathbb{Z}_2 gauge flux. In other words, it preserves the anomalous 1-form symmetry, with generators $W_p^f = \prod_{(ij) \in p} \sigma_1^z \sigma_2^y \sigma_3^x \sigma_4^z \sigma_5^y \sigma_6^x$ [98]. Therefore, the resulting mixed states must be LRE, and support deconfined fermionic excitations. In the maximally decohered case $p_f = \frac{1}{2}$, the f particles are heated to infinite temperature, so all of the three ground-state phases will end up in the maximally mixed state in the zero-flux sector ($W_p^f = 1, \forall p$), which belongs to the same intrinsic mixed-state quantum TO as that constructed in Section II. Actually, at $p_f = \frac{1}{2}$, this state can be obtained by applying a Hadamard gate on all vertical links to (11). Therefore, the decohered honeycomb model constructed here is also characterized by a nonzero TEN. We note that a similar model in the context of Lindblad equations was constructed in [99], but the LRE nature was not uncovered.

B. Decohered double semion model

As another example, we construct intrinsic mixed-state quantum TO from the double semion TO. The anyon content of the double semion TO is $\mathcal{A} = \{1, s, \bar{s}, s\bar{s}\} = \{1, s\} \times \{1, \bar{s}\}$, where s is a semion, $\theta(s) = i$; \bar{s} is an antiseimion, $\theta(\bar{s}) = -i$; and $s\bar{s}$ is a boson, $\theta(s\bar{s}) = 1$. The fusion rules are $s \times s = 1, \bar{s} \times \bar{s} = 1, s \times \bar{s} = s\bar{s}$ [100]. Following the general strategy in Section III, we can proliferate the semion s using noisy channels, and due to the trivial

braiding between s and \bar{s} , the 1-form symmetry generated by \bar{s} is preserved. Thus \bar{s} remains a strongly deconfined excitation with well-defined anti-semionic statistics.

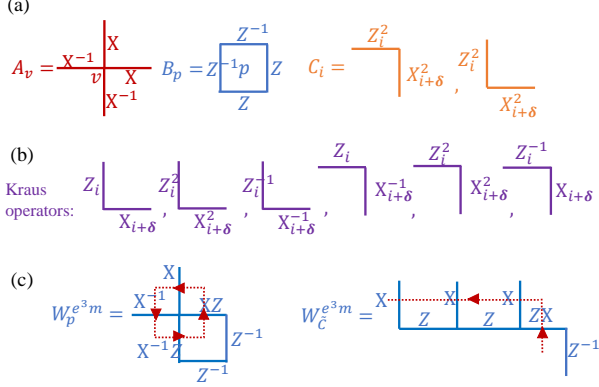


FIG. 6. (a). The stabilizers used in defining $H_{\mathbb{Z}_4 \text{ TC}}$ and H_{DS} . (b). The Kraus operators in the decohered double semion model. They are the shortest string operators of $[em]$ anyons. (c). A shortest closed $e^3 m$ string, $W_p^{e^3 m}$, and an open $e^3 m$ string $W_C^{e^3 m}$.

For concreteness, we start with the Pauli stabilizer model realizing the double semion TO [101]. The model is defined on a 2D square lattice with a \mathbb{Z}_4 degree of freedom on each link, which is equipped with the Pauli operators $Z = \sum_{n \in \mathbb{Z}_4} i^n |n\rangle\langle n|$ and $X = \sum_{n \in \mathbb{Z}_4} |n+1\rangle\langle n|$. The stabilizer model is defined as follows:

$$H_{\text{DS}} = - \sum_p (A_{v=p-\delta} B_p^{-1} + h.c.) - \sum_p B_p^2 - \sum_i C_i, \quad (27)$$

where A_v, B_p, C_i are represented graphically in Fig.6(a). Below we briefly review how this model is constructed from a parent \mathbb{Z}_4 toric code:

$$H_{\mathbb{Z}_4 \text{ TC}} = - \sum_v A_v - \sum_p B_p + h.c. \quad (28)$$

The anyon content of the \mathbb{Z}_4 toric code is $\{e^n m^r (n, r = 0, 1, 2, 3)\}$ with a $\mathbb{Z}_4 \times \mathbb{Z}_4$ fusion rule, $e^4 = m^4 = 1$. The statistics of the sixteen anyons are given by $\theta(e^n m^r) = i^{nr}$. The double semion TO described by H_{DS} is obtained by condensing the boson $e^2 m^2$ in the \mathbb{Z}_4 toric code (the C_i term is the shortest string operator of $e^2 m^2$, leading to its condensation), which causes confinement of anyons with nontrivial braiding with $e^2 m^2$ and identification of anyons related by fusion with $e^2 m^2$. Namely, $[a] = [a \times e^2 m^2]$ in the condensed theory, where we use $[a]$ to label the remaining deconfined anyons after the $e^2 m^2$ condensation. The deconfined anyons in the condensed theory are $\{[1], [em], [e^3 m], [e^2]\} = \{[1], [em]\} \times \{[1], [e^3 m]\}$, where $[em]$ is a semion and $[e^3 m]$ is an anti-semion. Indeed, a double semion TO is realized.

Next, we investigate the effect of proliferating $[em]$

anyons using the following quantum channel,

$$\mathcal{N}^{[em]} = \prod_i \mathcal{N}_i^{[em]}, \quad \mathcal{N}_i^{[em]}[\cdot] \equiv \sum_{n=0,1,2,3} p_n K_i^n \cdot K_i^{n\dagger} \quad (29)$$

The Kraus operators K_i, K_i^\dagger are the shortest string operators of $[em]$:

$$K_i = \begin{cases} Z_i X_i & \text{for vertical link } i \\ Z_i X_i^{-1} & \text{for horizontal link } i \end{cases} \quad (30)$$

For simplicity, we take the initial state ρ_0 to be the maximally mixed state in the ground-state subspace of H_{DS} and directly consider maximally decohered case $p_0 = p_1 = p_2 = p_3 = \frac{1}{4}$. Based on the analysis at the beginning of this section, it seems only the anti-semion $[e^3 m]$ will remain strongly deconfined, which leads to a chiral anti-semion theory $\{1, [e^3 m]\}$. However, the actual situation turns out to be even more intriguing.

First, we note that the 1-form symmetry generated by $e^3 m$ is indeed preserved because $[W_\gamma^{e^3 m}, K_i] = 0$, for any closed $e^3 m$ strings, which implies that $e^3 m$ is a deconfined anyon. Examples of a shortest closed $e^3 m$ string as well as an open $e^3 m$ string is given in Fig.6(c). On the other hand, the C_i terms in H_{DS} do not commute with the Kraus operators. As a result, for any open $e^2 m^2$ string $W_C^{e^2 m^2} = \prod_{i \in C} C_i$, $\text{tr}(\rho W_C^{e^2 m^2})$ becomes 0 for $\rho = \mathcal{N}^{[em]}[\rho_0]$. This means that the $e^2 m^2$ anyons are revived from the Bose-Einstein condensate and become a detectable anyon. Notably, the $e^2 m^2$ still proliferate classically, which is very different from Bose-Einstein condensation as we noted previously. Moreover, due to the strong 1-form symmetry generated by $e^3 m$ and the fusion rule $e^3 m \times e^3 m = e^2 m^2$, $e^2 m^2$ must become a deconfined anyon. Therefore, the remaining strongly deconfined anyons in ρ form a \mathbb{Z}_4 group $\{1, e^3 m, e^2 m^2, em^3\}$. We note that $e^3 m$ and em^3 are both anti-semions and $e^2 m^2$ is a transparent boson, meaning that it has trivial braiding with all strongly deconfined anyons. Anyon theories with transparent anyons are known as non-modular anyon theories [75, 102]. It is widely believed that non-modular anyon theories cannot be realized by local gapped Hamiltonians in 2D bosonic systems [97, 103]. This implies the lack of a pure-state counterpart of the mixed-state TO; thus it is indeed intrinsically mixed. Notably, the intrinsic mixed-state quantum TO constructed in Section II is also non-modular, with strongly deconfined anyons $\{1, f\}$. One crucial difference is that here the intrinsic mixed-state quantum TO does have a quantum memory. The undamaged part of the stored information is manipulated by the logical operators shown in Fig.7.

$$W_{\tilde{\gamma}_x}^{e^3 m} = \prod_{i \in \tilde{\gamma}_x} X_i Z_{i+\delta}, \quad W_{\tilde{\gamma}_y}^{e^3 m} = \prod_{i \in \tilde{\gamma}_y} X_i Z_{i+\delta}^{-1} \quad (31)$$

$W_{\tilde{\gamma}_x}^{e^3 m} W_{\tilde{\gamma}_y}^{e^3 m} = -W_{\tilde{\gamma}_y}^{e^3 m} W_{\tilde{\gamma}_x}^{e^3 m}$ as a consequence of the nontrivial self-braiding statistics of $e^3 m$. Besides, both $(W_{\tilde{\gamma}_x}^{e^3 m})^2, (W_{\tilde{\gamma}_y}^{e^3 m})^2$ are elements of the stabilizer group

defined by H_{DS} , thus acting trivially in the code space. Therefore, the intrinsic mixed-state quantum TO supports quantum memory with one and only one logical qubit. Remarkably, the anyon theory here is identi-

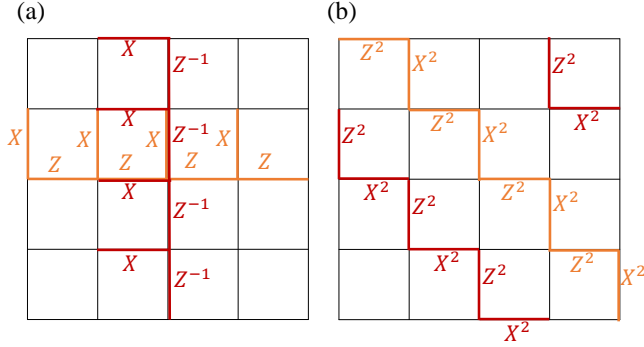


FIG. 7. (a). Two logical operators $W_{\gamma_x}^{e^3 m}$ (in orange) and $W_{\gamma_y}^{e^3 m}$ (in red). (b). Two non-local stabilizers. In both (a) and (b), periodic boundary conditions are imposed.

cal to the one obtained by incoherently proliferating the $em, e^2 m^2, e^3 m^3$ in the \mathbb{Z}_4 toric code via the same channel $\mathcal{N}^{[em]}$ [104, 105]. The relation between \mathbb{Z}_4 toric code, double semion, and the non-modular anyon theory is summarized in Fig. 8. However, it does not imply the final mixed states in the two models to be identical. Actually, the decohered \mathbb{Z}_4 toric code model (under $\mathcal{N}^{[em]}$) is fully characterized by the stabilizer group $G_{e^3 m} = \{\{W_p^{e^3 m}\}\}$, which defines the code space \mathcal{H}_C :

$$\mathcal{H}_C = \{|\psi\rangle, g|\psi\rangle = |\psi\rangle, \forall g \in G_{e^3 m}\} \quad (32)$$

In the maximally decohered case, the final state is the maximally mixed state in \mathcal{H}_C . For the decohered double semion model, however, there are additional non-local stabilizers formed by products of C_i . Two such non-local stabilizers are depicted in Fig. 7, and others non-local stabilizers can be obtained from these two via translation along the horizontal direction.

We summarize several surprising features of intrinsic mixed-state quantum TO revealed by this example. First, novel non-modular TO beyond the usual unitary modular tensor category description of 2+1D TO can be easily realized by Pauli stabilizer models under decoherence [104, 105]. Secondly, decoherence can sometimes give rise to new types of deconfined anyons that is absent in the anyon theory supported by the ground-state TO. It further implies that some features of the mixed-state TO can go beyond the prediction based on the anyon data, including the field-theoretic description [32, 33].

V. DISCUSSION

Our work introduces a promising mechanism for creating novel topologically ordered phases in mixed states.

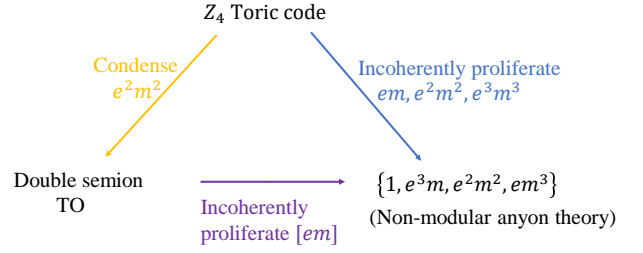


FIG. 8. Relations between \mathbb{Z}_4 toric code, double semion, and the non-modular anyon theory supported by intrinsic mixed-state quantum TO.

We give two complementary perspectives to demonstrate such possibility. The first perspective is to look at what anyons are proliferated. One of our key observations is that while the ways of anyon condensation are limited for pure states, anyon proliferation in mixed states can occur in more general ways, offering new possibilities for topological order. In the three models studied in this work, we propose new types of topological order arising from incoherent proliferation of fermionic or semionic anyons in ground-state topological order, which drives an unconventional phase transition that does not resemble any anyon condensation transition in pure states. The other perspective is to look at what remains. We find that the existence of anomalous strong 1-form symmetries can be viewed as a guiding principle to novel mixed-state TO. We give a general proof that anomalous strong 1-form symmetries implies the LRE nature of the mixed states, which manifests as deconfined anyons with nontrivial statistics. By analyzing the fusion rules and statistics of deconfined anyons, we show the possibility of realizing non-modular quantum TO in mixed states.

As is clear from the three examples, intrinsic mixed-state quantum TO can have or not have quantum memory, depending on whether the remaining deconfined anyons have nontrivial braiding statistics or only fermionic statistics [32].

It is worth noting that the construction of such exotic mixed states is experimentally feasible in current NISQ devices [17]. For example, one can realize the decohered \mathbb{Z}_2 toric code model in Section II by implementing incomplete error correction, where only the error syndrome with $A_v B_{p=v+\delta} = -1$ is corrected after the syndrome measurement using string operators W^e or W^m . This partial error correction would lead to a mixed state similar to ρ_f .

We end with some open directions. Firstly, as already mentioned in Section III, it remains unclear whether 1-form symmetries generated by fermions also guarantee bipartite long-range entanglement, or there exist counterexamples which are bipartite separable but have multipartite long-range entanglement [66]. Secondly, a systematic classification of the intrinsic mixed-state quantum TO is still lacking, with two main difficulties. The

first is how to treat the weakly deconfined anyons with the peculiar one-way braiding statistics. The other is how to generalize the discussion of anyon statistics to mixed states away from the fixed-point models, like the one discussed in [IID](#). Thirdly, it will be interesting to generalize our construction to get non-Abelian intrinsic mixed-state quantum TO, of which a simple route is to proliferate a subset of Abelian anyons in a known non-Abelian TO. The more intriguing case is to proliferate the non-Abelian anyons, in which case the decoherence-induced transition can be much harder to analyze. Finally, in our construction, we start from a topologically ordered state and get its descendants via noisy channels. It is also tempting to find systematic ways to prepare mixed-state topological order from short-range entangled mixed states, for example, by measuring mixed-state symmetry protected

topological order [[15](#), [29](#), [30](#), [34](#), [35](#)].

ACKNOWLEDGMENTS

Acknowledgments.—We are especially grateful to Ruihua Fan for many pieces of valuable advice and feedback on the manuscript. We also thank Tsung-Cheng Lu for pointing out to us the dependence of TEN on the choice of entanglement cut. We thank Yingfei Gu, Meng Cheng, Yu-An Chen, Zhen Bi, Jing-Yuan Chen, and He-Ran Wang for helpful discussions. This work is supported by NSFC under Grant No. 12125405. Zhengzhi Wu acknowledges the support of the Shuimu Fellow Foundation at Tsinghua University.

Appendix A: Details about the decohered toric code

1. Calculation of the coherent information and mapping to the RBIM

In this section, we present detailed calculation of the coherent information $I_c = S(\rho_f) - S(\rho_{Rf})$, and the derivation of the mapping to the RBIM along the Nishimori line ([\(4\)](#)) [[69](#)]. In the next two subsections, we calculate the two von Neumann entropy $S(\rho_f)$ and $S(\rho_{Rf})$ respectively, using the replica trick: $S = -\text{Tr}(\rho \log \rho) = -\lim_{n \rightarrow 1} \frac{\partial}{\partial n} \text{Tr}(\rho^n)$.

a. von Neumann entropy $S(\rho_{Rf})$

We begin with the calculation of $S(\rho_{Rf})$. We introduce 2 reference qubits, denoted by $\sigma_{1,2}$, and maximally entangle them with the two logical qubits in the ground state subspace of the system:

$$|\Psi\rangle = \frac{1}{2} \sum_{a,b=\pm 1} |a,b\rangle_S \otimes |\sigma_1^z = a, \sigma_2^z = b\rangle_R, \quad (\text{A1})$$

where a, b label the eigenvalues of the two non-contractible Wilson loops $W_{\gamma_x}^z, W_{\gamma_y}^z$ respectively, with the $U(1)$ phase ambiguity fixed by

$$|-1, 1\rangle_S = W_{\gamma_y}^x |1, 1\rangle_S, \quad |1, -1\rangle_S = W_{\gamma_x}^x |1, 1\rangle_S, \quad |-1, -1\rangle_S = W_{\gamma_y}^x W_{\gamma_x}^x |1, 1\rangle_S, \quad (\text{A2})$$

where $W_{\gamma_{x,y}}^x$ are non-contractible X loops on the dual lattice. It is straightforward to check that $|\Psi\rangle$ is a purification of ρ_0 , the maximally mixed state in the ground-state subspace, $\rho_0 = \text{tr}_R(|\Psi\rangle\langle\Psi|)$. One can alternatively view the reference qubits as an input (via the Choi map), which encodes information into the code space [[31](#)].

To facilitate the calculation of the coherent information, we write the decohered ρ_{Rf} in the error chain representation:

$$\rho_{Rf} = \sum_C P(C) W_C^f |\Psi\rangle\langle\Psi| W_C^f \quad (\text{A3})$$

where C stands for error chain configurations (the set of links where error occurs) with total length $|C|$. $P(C) = p^{|C|}(1-p)^{N-|C|}$ is the occurrence probability of the error chain C [[106](#)]. W_C^f is the (product of) open string operators which create f anyons at the ends of the C .

Now the trace $\text{Tr}(\rho_{Rf}^n)$ is,

$$\begin{aligned} \text{Tr}(\rho_{Rf}^n) &= \sum_{\{C^{(s)}\}} \prod_{s=1}^n P(C^{(s)}) \text{tr} \left[\prod_{s=1}^n \left(W_{C^{(s)}}^f |\Psi\rangle\langle\Psi| W_{C^{(s)}}^f \right) \right], \\ &= \sum_{\{C^{(s)}\}} \prod_{s=1}^n P(C^{(s)}) \langle\Psi| W_{C^{(s)}}^f W_{C^{(s+1)}}^f |\Psi\rangle, \end{aligned} \quad (\text{A4})$$

where $W_{C^{(n+1)}}^f \equiv W_{C^{(1)}}^f$ and the loops $C^{(s)}$ satisfy

$$C^{(s+1)} = C^{(1)} + \partial v^{(s)}, \quad s = 1, 2, \dots, n-1 \quad (\text{A5})$$

to give nonzero contribution. $\partial v^{(s)}$ are boundaries of a set of plaquettes $v^{(s)}$, so they are homologically trivial loops. Then $\text{Tr}(\rho_{Rf}^n)$ can be further simplified as

$$\text{Tr}(\rho_{Rf}^n) = \frac{1}{2^{n-1}} \sum_{C^{(1)}} P(C^{(1)}) \sum_{\{v^{(s)}\}} \prod_{s=1}^{n-1} P(C^{(1)} + \partial v^{(s)}). \quad (\text{A6})$$

The prefactor $\frac{1}{2^{n-1}}$ is due to the fact that for each replica $s = 1, 2, \dots, n-1$, there are two plaquette sets $v^{(s)}$ giving the same boundary $\partial v^{(s)}$. $\text{Tr}(\rho_{Rf}^n)$ can be mapped to the partition function of a classical Ising model with $n-1$ flavors of Ising spin and a defect line at C^1 . Concretely, we introduce Z_2 variables $n_{v^{(s)}}(l) = 1, 0$ to denote whether link l is occupied in $\partial v^{(s)}$ or not. Then we can express the probability $P(C^{(1)} + \partial v^{(s)})$ by the Z_2 variables $n_{v^{(s)}}(l)$. For example, if a link $l \in C^{(1)}$ and $n_{v^{(s)}}(l) = 1$, then link l does not occur in the error chain $C^{(1)} + \partial v^{(s)}$ and contributes a factor $(1-p)^{n_{v^{(s)}}(l)} p^{1-n_{v^{(s)}}(l)}$ in $P(C^{(1)} + \partial v^{(s)})$. As a result, the probability $P(C^{(1)} + \partial v^{(s)})$ can be written as

$$P(C^{(1)} + \partial v^{(s)}) = [\prod_{l \in C^{(1)}} ((1-p)^{n_{v^{(s)}}(l)} p^{1-n_{v^{(s)}}(l)})] [\prod_{l \notin C^{(1)}} (p^{n_{v^{(s)}}(l)} (1-p)^{1-n_{v^{(s)}}(l)})]. \quad (\text{A7})$$

The first part with those links belonging to the error chain $C^{(1)}$ can be made symmetric as

$$\begin{aligned} \prod_{l \in C^{(1)}} ((1-p)^{n_{v^{(s)}}(l)} p^{1-n_{v^{(s)}}(l)}) &= \prod_{l \in C^{(1)}} \left(\sqrt{p(1-p)} \left(\frac{1-p}{p} \right)^{n_{v^{(s)}}(l) - \frac{1}{2}} \right) \\ &= \sqrt{p(1-p)}^{|C^{(1)}|} \prod_{l \in C^{(1)}} \left(\frac{1-p}{p} \right)^{n_{v^{(s)}}(l) - \frac{1}{2}}. \end{aligned} \quad (\text{A8})$$

Similarly, we also make the second part symmetric as

$$\begin{aligned} \prod_{l \notin C^{(1)}} (p^{n_{v^{(s)}}(l)} (1-p)^{1-n_{v^{(s)}}(l)}) &= \prod_{l \notin C^{(1)}} \left(\sqrt{(1-p)p} \left(\frac{p}{1-p} \right)^{n_{v^{(s)}}(l) - \frac{1}{2}} \right) \\ &= \sqrt{p(1-p)}^{(N-|C^{(1)}|)} \prod_{l \notin C^{(1)}} \left(\frac{p}{1-p} \right)^{n_{v^{(s)}}(l) - \frac{1}{2}}. \end{aligned} \quad (\text{A9})$$

Then we can express the link probability part $(\frac{p}{1-p})^{n_{v^{(s)}}(l) - \frac{1}{2}}$ or $(\frac{1-p}{p})^{n_{v^{(s)}}(l) - \frac{1}{2}}$ as an Ising coupling between two nearest-neighbour plaquettes which share the link l . Concretely, we introduce $n-1$ flavours of Ising spins $\tau^{(s)} = \pm 1, s = 1, 2, \dots, n-1$ on each plaquette, and introduce the Ising coupling constant J as: $e^{-2J} = p/(1-p)$. Then the link probability part $(\frac{p}{1-p})^{n_{v^{(s)}}(l) - \frac{1}{2}}$ or $(\frac{1-p}{p})^{n_{v^{(s)}}(l) - \frac{1}{2}}$ can be written as $\exp[J\eta_{ij}\tau_i^{(s)}\tau_j^{(s)}]$, where i, j are the dual lattice site coordinates of the two plaquettes, and $\eta_{ij} = -1$ (1) for l belonging to (not belonging to) the error chain $C^{(1)}$. Then p is the probability of antiferromagnetic coupling for each bond.

As a result, $\text{Tr}(\rho_{Rf}^n)$ can be expressed as the partition function of a random bond Ising model (RBIM) with $n-1$ flavours of Ising spins and periodic boundary condition (PBC):

$$\begin{aligned} \text{Tr}(\rho_{Rf}^n) &= \frac{1}{2^{n-1}} \sum_{C^{(1)}} P(C^{(1)}) \sum_{\{v^{(s)}\}} \prod_{s=1}^{n-1} P(C^{(1)} + \partial v^{(s)}) \\ &= \frac{1}{2^{n-1}} \left(\sqrt{(1-p)p} \right)^{(n-1)N} \sum_{C^{(1)}} P(\{\eta\}) \sum_{\{\tau^{(s)}\}} \prod_{s=1}^{n-1} \exp[J\eta_{ij}\tau_i^{(s)}\tau_j^{(s)}] \\ &= \frac{1}{2^{n-1}} \left(\sqrt{(1-p)p} \right)^{(n-1)N} \sum_{C^{(1)}} P(\{\eta\}) \prod_{s=1}^{n-1} \sum_{\{\tau^s\}} \exp[J\eta_{ij}\tau_i^{(s)}\tau_j^{(s)}] \\ &= \frac{1}{2^{n-1}} \left(\sqrt{(1-p)p} \right)^{(n-1)N} \sum_{C^{(1)}} P(\{\eta\}) (Z[J, \{\eta\}])^{n-1}. \end{aligned} \quad (\text{A10})$$

Finally we take the replica limit $n \rightarrow 1$ to derive the von Neumann entropy $S(\rho_{Rf})$:

$$\begin{aligned} S(\rho_{Rf}) &= -\lim_{n \rightarrow 1} \frac{\partial}{\partial n} \text{Tr}(\rho_{Rf}^n) \\ &= -\frac{N}{2} \log[p(1-p)] + \log 2 - \sum_{\{\eta\}} P(\{\eta\}) \log Z[J, \{\eta\}] \\ &\equiv -\overline{\log Z_{\text{PBC}}^{\text{RBIM}}} + \log 2 - \frac{N}{2} \log[p(1-p)], \end{aligned} \quad (\text{A11})$$

where the first term is the average free energy of the RBIM along the Nishimori line: $e^{-2J} = \frac{p}{1-p}$.

b. von Neumann entropy $S(\rho_f)$

The von Neumann entropy $S(\rho_f)$ can be derived similar to $S(\rho_{Rf})$. The initial density matrix is

$$\rho_0 = \frac{1}{4} \sum_{a,b=\pm 1} |a,b\rangle\langle a,b|. \quad (\text{A12})$$

Then $\text{Tr}(\rho_f^n)$ is

$$\begin{aligned} \text{Tr}(\rho_f^n) &= \sum_{\{C^{(s)}\}} \sum_{a^{(s)}, b^{(s)}} \prod_{s=1}^n P(C^{(s)}) \left(\frac{1}{4} \langle a^{(s)}, b^{(s)} | W_{C^{(s)}}^f W_{C^{(s+1)}}^f | a^{(s+1)}, b^{(s+1)} \rangle \right) \\ &= \frac{1}{2^{n-1}} \cdot \frac{1}{4^{n-1}} \sum_{C^{(1)}} P(C^{(1)}) \prod_{s=1}^{n-1} \sum_{\{v^{(s)}\}} \sum_{d_x^{(s)}, d_y^{(s)}=0,1} P(C^{(1)} + \partial v^{(s)} + d_x^{(s)} \gamma_x + d_y^{(s)} \gamma_y), \end{aligned} \quad (\text{A13})$$

where $n+1 \equiv 1$, and $d_{x,y}^{(s)} = 0,1$ denotes whether or not $C^{(s)}$ lies in the same homological class as $C^{(1)}$. Similar to the mapping of $\text{Tr}(\rho_{Rf}^n)$ to the partition function of RBIM, we can also map $\text{Tr}(\rho_f^n)$ to the partition function of RBIM, except that here we must sum over the four contributions of inserting or not the two non-contractible defect lines on the torus:

$$\begin{aligned} \text{Tr}(\rho_f^n) &= \frac{1}{2^{n-1}} \cdot \frac{1}{4^{n-1}} \left(\sqrt{(1-p)p} \right)^{(n-1)N} \sum_{C^{(1)}} P(\{\eta\}) \left(\sum_{d_x, d_y=0,1} Z_{d_x, d_y}[J, \{\eta\}] \right)^{n-1} \\ &\equiv \frac{1}{2^{n-1}} \cdot \frac{1}{4^{n-1}} \left(\sqrt{(1-p)p} \right)^{(n-1)N} \left(\sum_{d_x, d_y=0,1} Z_{d_x, d_y}^{\text{RBIM}} \right)^{n-1} \end{aligned} \quad (\text{A14})$$

where $Z_{d_x, d_y}^{\text{RBIM}}$ is the partition function with d_a non-contractible defect lines inserted along the cycle γ_a . Along the defect line the coupling changes from ηJ to $-\eta J$. This is equivalent to taking the anti-periodic boundary condition (APBC).

S_{ρ_f} can in turn be obtained by taking the replica limit:

$$S(\rho_f) = -\lim_{n \rightarrow 1} \frac{\partial}{\partial n} \text{Tr}(\rho_f^n) = 3 \log 2 - \log \left[\overline{\sum_{d_x, d_y=0,1} Z_{d_x, d_y}^{\text{RBIM}}} \right] - \frac{N}{2} \log[p(1-p)]. \quad (\text{A15})$$

We note that the second term can also be understood as the free energy of RBIM with all four types of boundary condition (PBC/APBC along x, y direction) into account.

c. Critical error rate and classical memory from coherent information

As we have demonstrated in the previous subsections, S_{ρ_f} and $S_{\rho_{Rf}}$ can be mapped to the free energy of the RBIM with or without the insertion of non-contractible defect lines (plus some constants), so the coherent information I_c is related the excess free energy of the defect line,

$$I_c = 2 \log 2 - \log \frac{\sum_{d_x, d_y=0,1} Z_{d_x, d_y}^{\text{RBIM}}}{Z_{00}^{\text{RBIM}}} = 2 \log 2 - \log \left[\sum_{d_x, d_y=0,1} e^{-\Delta F_{d_x, d_y}} \right], \quad (\text{A16})$$

where $\Delta F_{d_x, d_y}$ is the excess free energy with the insertion of a non-contractible defect line. For small p , the RBIM is in the ferromagnetic (FM) phase, and the excess free energy of a defect line is extensive, $\Delta F_{\{d_x, d_y\} \neq \{0,0\}} \sim O(L)$, which leads to $I_c = 2 \log 2$. On the other hand, when p is above the error threshold $p_c \approx 0.109$, the RBIM undergoes a phase transition to a paramagnetic (PM) phase, and $I_c < 2 \log 2$. This is exactly the same as the situation with single-qubit errors. The classical memory of ρ_f is also reflected in the fact that $I_c \geq 0$.

2. Relative entropy

As mentioned in the main text, the phase transition at $p_f = p_c$ is driven by the proliferation of f anyons. In the double space, this corresponds to the condensation of $f_+ f_-$. In this section we provide a quantitative diagnosis of the f anyon proliferation in the original Hilbert space. We denote the string operators creating α anyons at the ends of the string as w^α , and investigate whether $\rho_f^\alpha \equiv \mathcal{N}^f [w^\alpha \rho_0 w^\alpha]$ is really a distinct state from ρ_f . Quantitatively, we calculate the relative entropy:

$$D(\rho_f \| \rho_f^\alpha) \equiv \text{Tr}(\rho_f \log \rho_f) - \text{Tr}(\rho_f \log \rho_f^\alpha), \quad (\text{A17})$$

and examine whether it diverges as the length of w^α approaches infinity, which is proposed as a generalization of Fredenhagen-Marcu order parameter for ground states [31, 107, 108].

It turns out that, for $p_f < p_c$, $D(\rho_f \| \rho_f^\alpha)$ diverges for all three types of anyons, while for $p_f > p_c$, $D(\rho_f \| \rho_f^f)$ becomes finite, in agreement with our expectation. Additionally, although $D(\rho_f \| \rho_f^{e(m)})$ is divergent, e, m cease to be distinct (weakly) deconfined excitations since $e \times f = m$.

To obtain $D(\rho_f \| \rho_f^\alpha)$, we can still use the replica trick:

$$D^{(n)}(\rho_f \| \rho_f^\alpha) \equiv \frac{1}{1-n} \log \frac{\text{Tr} \rho_f (\rho_f^\alpha)^{n-1}}{\text{Tr} \rho_f^n}, \quad (\text{A18})$$

and recover $D(\rho_f \| \rho_f^\alpha)$ by taking the limit $n \rightarrow 1$.

Using the error chain expansion, we get

$$\begin{aligned} \text{Tr} \rho_f (\rho_f^\alpha)^{n-1} &= \sum_{\{C^{(s)}\}} \prod_{s=1}^n P(C^{(s)}) \text{Tr} \left(W_{C^{(1)}}^f \rho_0 W_{C^{(1)}}^f \prod_{s=2}^n W_{C^{(s)}}^f w^\alpha \rho_0 w^\alpha W_{C^{(s)}}^f \right) \\ &= \sum_{\{C^{(s)}\}} \sum_{a^{(s)}, b^{(s)}} \left[\prod_{s=1}^n \frac{1}{4} P(C^{(s)}) \right] \langle a^{(1)}, b^{(1)} | W_{C^{(1)}}^f W_{C^{(2)}}^f w^\alpha | a^{(2)}, b^{(2)} \rangle \langle a^{(n)}, b^{(n)} | w^\alpha W_{C^{(n)}}^f W_{C^{(1)}}^f | a^{(1)}, b^{(1)} \rangle \\ &\quad \prod_{s=2}^{n-1} \langle a^{(s)}, b^{(s)} | w^\alpha W_{C^{(s)}}^f W_{C^{(s+1)}}^f w^\alpha | a^{(s+1)}, b^{(s+1)} \rangle. \end{aligned} \quad (\text{A19})$$

Clearly, for $\alpha = e, m$, $\text{Tr} \rho_f (\rho_f^\alpha)^{n-1} = 0$, so the relative entropy diverges. Thus we only focus on $\alpha = f$ next. Terms in the summation is nonvanishing only if the error chain configurations satisfy the following condition:

$$C^{(s)} = C^{(1)} + \partial v^{(s)} + d_x^{(s)} \gamma_x + d_y^{(s)} \gamma_y + A, \quad s = 1, 2, \dots, n-1, \quad (\text{A20})$$

where $d_{x/y}^{(s)} = 0, 1$ and A denotes the string where $w^{\alpha=f}$ acts nontrivially. Compared to (A13), (A14), we can see that the insertion of w_A^f corresponds to inserting an additional defect line along A in the RBIM, which means the Ising coupling flips sign along A . Denote the partition function of RBIM with defect line along A as $Z^{\text{RBIM}}[A]$, where we implicitly sum over the four types of boundary conditions $\{d_x, d_y\}$. Then

$$D^{(n)}(\rho_f \| \rho_f^f) = \frac{1}{1-n} \log \frac{\overline{(Z^{\text{RBIM}}[A])^{n-1}}}{\overline{(Z^{\text{RBIM}})^{n-1}}}, \quad (\text{A21})$$

Taking the replica limit $n \rightarrow 1$, we obtain the relative entropy:

$$D(\rho_f \| \rho_f^f) = \overline{\log Z^{\text{RBIM}}} - \overline{\log Z^{\text{RBIM}}[A]}, \quad (\text{A22})$$

which is mapped to the excess free energy of defect line A . In the FM phase ($p < p_c$), it diverges as the distance between the two ends of A goes to infinity. However, in the PM phase ($p > p_c$), it is finite, which indicates the incoherent proliferation of f .

3. Calculation of the entanglement negativity

In this section, we derive the entanglement negativity $\varepsilon_A(\rho_f) \equiv \log \|\rho_f^{T_A}\|_1$. It turns out that to calculate $\varepsilon_A(\rho_f)$, it is more convenient to use the loop expansion ((7) in the main text) instead of the error chain expansion used in the last two sections. We start from (9) in the main text:

$$\rho_f^{T_A} = \frac{1}{2^N} \sum_{g \in G} (1-2p)^{l_g} y_A(g) g, \quad (\text{A23})$$

where l_g is the length of the segment where g_x and g_z does not coincidence, and

$$y_A(g) \equiv \text{sign}_A(g_x, g_z) \equiv \begin{cases} 1, & \text{if } g_{xA}, g_{zA} \text{ commute.} \\ -1, & \text{if } g_{xA}, g_{zA} \text{ anticommute.} \end{cases}$$

To calculate $\varepsilon_A(\rho_f)$, we utilize the replica trick, that is, we first calculate the $2n^{\text{th}}$ Renyi negativity $\varepsilon_A^{(2n)}(\rho_f) := \frac{1}{2-2n} \log \frac{\text{Tr}(\rho_f^{T_A})^{2n}}{\text{Tr}\rho_f^{2n}}$ and finally take the replica limit $2n \rightarrow 1$.

First, we consider the bipartition of $A \cup \bar{A}$ of a cylinder, as shown in Fig. 1 (g)-(i) in the main text. We denote the bipartition in Fig. 1(h) as bipartition 1 and that in Fig. 1(i) as bipartition 2. We discuss these two types of bipartitions in detail below.

Bipartition 1, generic p . We deal with bipartition 1 first. In this case we are able to obtain an exact result of $\varepsilon_A^{(2n)}$ for any p . As we will show below, the result actually does not depend on p at all. To start with, we calculate $(\rho_f^{T_A})^2$,

$$\begin{aligned} (\rho_f^{T_A})^2 &= \frac{1}{2^{2N}} \sum_{g, h \in G} (1-2p)^{l_g + l_h} y_A(g) y_A(h) gh \\ &= \frac{1}{2^{2N}} \sum_{g, h \in G} (1-2p)^{l_g + l_h} y_A(gh) \text{sign}_A(g, h) gh \\ &= \frac{1}{2^{2N}} \sum_{g, \tilde{g} \in G} (1-2p)^{l_g + l_{g\tilde{g}}} y_A(\tilde{g}) \text{sign}_A(g, \tilde{g}) \tilde{g}. \end{aligned} \quad (\text{A24})$$

In the last step we use the substitution $h = g\tilde{g}$.

To simplify the expression, we deal with the summation over g first. The crucial part in this expression is $\text{sign}_A(g, \tilde{g})$ which leads to complete destructive interference when \tilde{g} crosses the boundary between A, \bar{A} . To be more precise, we define the subgroup H of G :

$$H \equiv \{g \in G | g_A g'_A = g'_A g_A, \forall g' \in G\}. \quad (\text{A25})$$

For bipartition 1, H contains all loops that do not cross the boundary. Then we can simplify (A24) :

$$(\rho_f^{T_A})^2 = \frac{1}{2^{2N}} \sum_{g \in G, \tilde{g} \in H} (1-2p)^{l_g + l_{g\tilde{g}}} y_A(\tilde{g}) \tilde{g}. \quad (\text{A26})$$

Thus

$$\begin{aligned} \text{Tr}(\rho_f^{T_A})^{2n} &= 2^{-2nN} \prod_{s=1}^n \sum_{\tilde{g}^{(s)} \in H} \prod_{s=1}^n \sum_{g^{(s)} \in G} (1-2p)^{\sum_{s=1}^n l_{g^{(s)}} + l_{g^{(s)}\tilde{g}^{(s)}}} y_A(\prod_{s=1}^n \tilde{g}^{(s)}) \text{Tr} \left(\prod_{s=1}^n \tilde{g}^{(s)} \right) \\ &= 2^{(1-2n)N} \sum_{\tilde{g}^{(1)}, \dots, \tilde{g}^{(n-1)} \in H} \sum_{g^{(1)}, \dots, g^{(n)} \in G} (1-2p)^{\sum_{s=1}^{n-1} (l_{g^{(s)}} + l_{g^{(s)}\tilde{g}^{(s)}}) + l_{\prod_{s=1}^{n-1} g^{(s)}} + l_{\prod_{s=1}^{n-1} g^{(s)}\tilde{g}^{(s)}}}. \end{aligned} \quad (\text{A27})$$

In a similar manner we can obtain $\text{Tr}\rho_f^{2n}$, resulting in a similar expression with the summation over H replaced by a summation over G :

$$\text{Tr}\rho_f^{2n} = 2^{(1-2n)N} \sum_{\tilde{g}^1, \dots, \tilde{g}^{n-1} \in G} \sum_{g^1, \dots, g^n \in G} (1-2p)^{\sum_{s=1}^{n-1} (l_{g^{(s)}} + l_{g^{(s)}\tilde{g}^{(s)}}) + l_{\prod_{s=1}^{n-1} g^{(s)}} + l_{\prod_{s=1}^{n-1} g^{(s)}\tilde{g}^{(s)}}}. \quad (\text{A28})$$

Since we are only concerned about their ratio, we can extract the common part in the expression and rename it as $O_{\{\tilde{g}\}}$.

$$O_{\{\tilde{g}\}} = 2^{(1-2n)N} \sum_{g^1, \dots, g^n \in G} (1-2p)^{\sum_{s=1}^{n-1} (l_{g^{(s)}} + l_{g^{(s)} \tilde{g}^{(s)}}) + l_{\prod_{s=1}^{n-1} g^{(s)}} + l_{\prod_{s=1}^{n-1} g^{(s)} \tilde{g}^{(s)}}}. \quad (\text{A29})$$

It is straightforward to show that $O_{\{\tilde{g}\}}$ is actually only a function of $l_{\tilde{g}^{(s)}}$. Based on this observation, we can divide the summation over $\{\tilde{g}\}$ into different classes. First, we define the invariant subgroup G_f of G , generated by $A_{v=p-\delta} B_p$. In other words, elements in G_f are tensionless loops with $l_g = 0$. Similarly, we define the subgroup H_f of H to be $H_f \equiv \{g \in G_f | g_A g'_A = g'_A g_A, \forall g' \in G_f\}$. Then

$$\begin{aligned} \text{Tr}(\rho_f^{TA})^{2n} &= \sum_{\tilde{g}_f^1, \dots, \tilde{g}_f^{n-1} \in H_f} \sum_{\tilde{u}^1, \dots, \tilde{u}^{n-1} \in H/H_f} O_{\{\tilde{u}\}}, \\ \text{Tr} \rho_f^{2n} &= \sum_{\tilde{g}_f^1, \dots, \tilde{g}_f^{n-1} \in G_f} \sum_{\tilde{u}^1, \dots, \tilde{u}^{n-1} \in G/G_f} O_{\{\tilde{u}\}} \end{aligned} \quad (\text{A30})$$

Since $G/G_f = H/H_f$, we get

$$\frac{\text{Tr}(\rho_f^{TA})^{2n}}{\text{Tr} \rho_f^{2n}} = \left(\frac{|H_f|}{|G_f|} \right)^{n-1} = 2^{(2-2n)(L-1)}, \quad (\text{A31})$$

where L is the length of the entanglement cut. Thus the Renyi negativity is:

$$\varepsilon_A^{(2n)}(\rho_f) = (L-1) \log 2, \forall n. \quad (\text{A32})$$

In the replica limit $2n \rightarrow 1$, we get $\varepsilon_A(\rho_f) = (L-1) \log 2$. The subleading term, $\log 2$, is the topological entanglement negativity (TEN), which takes exactly the same value as that of the toric-code ground state.

Bipartition 2, $p = \frac{1}{2}$. For bipartition 2, the calculation for generic p is much more challenging. This is mainly because $G/G_f \neq H/H_f$, which means (A31) cannot be derived from (A30) for generic p . As a result, the negativity does depend on p for this bipartition. Here we are mainly interested in the phase with intrinsic mixed-state quantum TO for $p > p_c$, so we take the maximally decohered limit, $p = \frac{1}{2}$, in which case the calculation can be greatly simplified.

For $p = \frac{1}{2}$,

$$\rho_f = \frac{1}{2^N} \sum_{g_f \in G_f} g_f = \frac{1}{2^{N/2+1}} \prod_p \frac{1+W_p}{2}, \quad W_p := A_{p-\delta} B_p. \quad (\text{A33})$$

In this case the negativity exhibits an unusual dependence on the parity of L , as shown in (12) in the main text. We will derive this result below.

Analogous to (A24) and (A26), we have,

$$\begin{aligned} (\rho_f^{TA})^2 &= \frac{1}{2^{2N}} \sum_{g_f, \tilde{g}_f \in G_f} y_A(\tilde{g}_f) \text{sign}_A(g_f, \tilde{g}_f) \tilde{g}_f \\ &= \frac{1}{2^{2N}} \sum_{g_f \in G_f, \tilde{g}_f \in H_f} y_A(\tilde{g}_f) \tilde{g}_f. \end{aligned} \quad (\text{A34})$$

Then it is straightforward to obtain the Renyi negativity:

$$\varepsilon_A^{(2n)}(\rho_f) = \frac{1}{2-2n} \log \left(\frac{|H_f|}{|G_f|} \right)^{n-1}. \quad (\text{A35})$$

For odd L , $\frac{|G_f|}{|H_f|}$ amounts to the number of elements in G_f acting on the boundary: $\frac{|G_f|}{|H_f|} = 2^{L-1}$. Here the “-1” is due to the fact that $h = \prod_{p_i \text{ on the boundary}} W_{p_i}$ is an element in H_f . Consequently, $\varepsilon_A^{(2n)}(\rho_f) = \frac{L-1}{2} \log 2$. The negativity is half the value for bipartition 1, because there are only a half number of W_p acting on the boundary.

For even L , the calculation is subtler. Specifically, there exist special elements $h_1 = \prod_{i=1,3,\dots,L-1} W_{p_i}$, $h_2 = \prod_{i=2,4,\dots,L} W_{p_i}$ ($= h \cdot h_1$), that acts nontrivially on the boundary, but still belongs to H_f . See Fig.9(a) for an illustration. Therefore, $\frac{|G_f|}{|H_f|} = 2^{L-2}$, $\varepsilon_A^{(2n)}(\rho_f) = \frac{L-2}{2} \log 2$.

Taking the replica limit $2n \rightarrow 1$, we get the final result of logarithmic negativity (for bipartition 2):

$$\varepsilon_A(\rho_f) = \begin{cases} \frac{L}{2} \log 2 - \log 2, & \text{if } L \text{ is even,} \\ \frac{L}{2} \log 2 - \frac{\log 2}{2}, & \text{if } L \text{ is odd.} \end{cases} \quad (\text{A36})$$

In all the cases, we get a nonzero TEN, indicating nontrivial topological order. Here the value of TEN exhibits an unusual dependence on the parity of boundary size, and thus seems to be less universal than we would expect for topologically ordered phase. In the next section we will try to resolve this puzzle by relating entanglement properties of ρ_f to those of more familiar ground-state topological order.

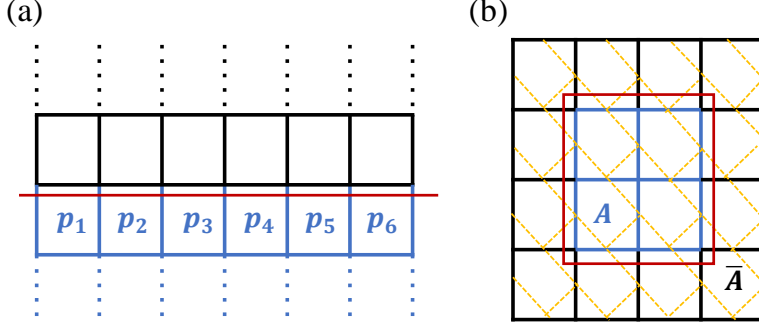


FIG. 9. (a). Bipartition 2 on a cylinder, $L = 6$ in this case. (b). An example of bipartition with contractible subregion A . Orange dashed lines represent auxiliary links. $N_l = 12$ in this case.

Before that, we first make some quick comments on entanglement negativity for more generic bipartitions, including the cases with contractible subregion A . For $p = \frac{1}{2}$, we can perform similar calculations above and get exact results of negativity with general bipartitions. It is convenient to introduce some auxiliary links connecting the six qubits acted upon by W_p for each p . We give one example in Fig. 9(b). With the help of these auxiliary links, the entanglement negativity for general bipartitions (with the only assumption that both A and \bar{A} are connected) yields,

$$\varepsilon_A(\rho_f) = \begin{cases} \frac{N_l}{2} \log 2 - \log 2, & \text{if } N_l \text{ is even,} \\ \frac{N_l}{2} \log 2 - \frac{\log 2}{2}, & \text{if } N_l \text{ is odd.} \end{cases} \quad (\text{A37})$$

N_l counts the number of auxiliary links that are cut through by the entanglement cut. The even/odd dependence shows up again. The reason that bipartition 1 is free of this problem is that $N_l = 2L$ is always even in that case. Finally, we note that due to the unusual dependence of TEN (defined as the value of the subleading term here) on the boundary size, one cannot extract TEN by calculating the tripartite mutual information as in the Kitaev-Preskill scheme, unless carefully choosing the multipartition such that N_l have the same parity for all subregions.

4. Relation to translation-symmetry-enriched \mathbb{Z}_2 TO

In this section we give an explanation of the curious dependence of TEN on the entanglement cut, by establishing a connection between the entanglement properties of ρ_f and ground-state \mathbb{Z}_2 topological order enriched by translation symmetry. To establish this connection, we first note that at $p = \frac{1}{2}$, ρ_f is nothing but the maximally mixed state with $W_p = A_{p-\delta} B_p = 1, \forall p$. To find its analog in ground states of local Hamiltonians, it is natural design a stabilizer code with W_p being the stabilizers. Of course, without other terms, we would get a very large ground state degeneracy, and the maximally mixed states in the ground state subspace is just ρ_f . Thus we need more stabilizers. Here we provide one illuminating choice:

$$H_{\text{SET}} = - \sum_p W_p - \sum_{\text{vertical link } i} Z_i X_{i+\delta}. \quad (\text{A38})$$

It is straightforward to check that all terms in the H_{SET} commute with each other, and the ground state is determined up to topological degeneracy. Actually, this model has been recently constructed and studied in [109]. We briefly summarize the important properties of this model: 1. It has Z_2 (toric-code) topological order, i.e., it has the same type of anyon excitations and same statistics as the toric code. 2. In this model the Z_2 topological order is enriched by translation symmetry along the horizontal direction, which is manifested in the fact that excitations $W_p = -1$ for p on even columns and odd columns belong to different anyon superselection sectors, and correspond to e and m anyons in the toric code, respectively. This phenomenon is often called weak symmetry breaking. 3. As a consequence of weak symmetry breaking, the ground state degeneracy (GSD) on a torus depend on the linear size along the horizontal direction, denoted by L_x : $\text{GSD} = 4(2)$ for even (odd) L_x .

Our primary goal for introducing this model is to understand the weird behavior of entanglement negativity (A39) of ρ_f for bipartition 2, so we consider putting the model (A38) on a cylinder and investigate the entanglement property of the ground state under the same bipartition. First, we note that the ground state, or more specifically, the maximally mixed state in the ground state subspace, can be written in an illuminating way: $\rho_{\text{GS}} \propto \rho_f \prod_{\text{vertical link } i} \frac{1+Z_i X_{i+\delta}}{2}$. Moreover, for bipartition 2, the entanglement cut does not go through the stabilizers $Z_i X_{i+\delta}$ at all, so these stabilizers contribute zero entanglement. Thus,

$$\varepsilon_A(\rho_{\text{GS}}) = \varepsilon_A(\rho_f) = \begin{cases} \frac{L_x}{2} \log 2 - \log 2, & \text{if } L_x \text{ is even,} \\ \frac{L_x}{2} \log 2 - \frac{\log 2}{2}, & \text{if } L_x \text{ is odd.} \end{cases} \quad (\text{A39})$$

We can instead calculate the entanglement entropy S_A for a (pure) ground state, with a bit more complication. To do this, we need to first specify the boundary condition at the upper and lower boundaries of the cylinder (nevertheless, the result does not depend on the choice of the boundary condition). Then by fixing the value of the logical string operators along the horizontal direction, we can get a pure state and calculate its bipartite entanglement entropy, which yields the same result:

$$S_A = \begin{cases} \frac{L_x}{2} \log 2 - \log 2, & \text{if } L_x \text{ is even,} \\ \frac{L_x}{2} \log 2 - \frac{\log 2}{2}, & \text{if } L_x \text{ is odd.} \end{cases} \quad (\text{A40})$$

Thus, the TEN of ρ_f can be directly related to the TEN/TEE of the ground state of H_{SET} . For the latter, the dependence of TEN/TEE on the parity of L_x is a common feature of topological order with weak symmetry breaking of translations, and can be understood in the following way: Since translations permute e and m , for odd L_x , e and m are exchanged when going around the cylinder (along the x direction) once. Thus instead of two independent logical string operators along the x direction as naively expected (for even L_x , the two logical string operators can be constructed by creating a pair of e or m anyons, dragging one of them around a cycle, and annihilating the pair), one can only find one. This subtlety here causes the TEE/TEN as well as the GSD only half the value as expected for the toric-code topological order.

5. Robustness under phase errors

In this section, we aim to discuss the robustness of the intrinsic mixed-state quantum topological order under other noises. We derive the phase diagram in Fig. 2 with additional single-qubit phase errors. Concretely, we consider the following mixed state:

$$\rho_{f,e} = \mathcal{N}^z \circ \mathcal{N}^f[\rho_0]. \quad (\text{A41})$$

Similar to section A, B, we analyze the property of $\tilde{\rho}_f$ by calculating the von Neumann entropy $S(\tilde{\rho}_f)$ and map it to statistical models.

We denote the error rate and error chain configuration of \mathcal{N}^z (\mathcal{N}^f) as p_z (p_f) and C_z (C_f), respectively. Then $\rho_{f,e}$ can be represented by error chain expansion as in (A3),

$$\rho_{f,e} = \sum_{C_z, C_f} P_f(C_f) P_z(C_z) W_{C_f}^f W_{C_z}^e \rho_0 W_{C_z}^e W_{C_f}^f. \quad (\text{A42})$$

Then we can write the n -th moment as

$$\text{Tr}(\rho_{f,e}^n) = \sum_{\{C^{(s)}\}} \sum_{a^{(s)}, b^{(s)}} \prod_{s=1}^n \frac{1}{4} P_f(C_f^{(s)}) P_z(C_z^{(s)}) \langle a^{(s)}, b^{(s)} | W_{C_z^{(s)}}^e W_{C_f^{(s)}}^f W_{C_f^{(s+1)}}^f W_{C_z^{(s+1)}}^e | a^{(s+1)}, b^{(s+1)} \rangle. \quad (\text{A43})$$

Nonzero contributions only come from error chain configurations satisfying

$$C_z^{(s)} = C_z^{(1)} + \partial v^{(s)} + d_x^{z,(s)}\gamma_x + d_x^{z,(s)}\gamma_y, \quad C_f^{(s)} = C_f^{(1)} + \partial v^{(s)} + d_x^{f,(s)}\gamma_x + d_x^{f,(s)}\gamma_y, \quad (\text{A44})$$

so (A43) can be simplified as:

$$\text{Tr}(\rho_{f,e}^n) = \frac{1}{4^{n-1}} \cdot \frac{1}{4^{n-1}} \prod_{\alpha=z,f} \left[\sum_{C_\alpha^{(s)}} P(C_\alpha^{(1)}) \prod_{s=1}^{n-1} \sum_{\{v_\alpha^{(s)}\}} \sum_{d_x^{\alpha,(s)}, d_y^{\alpha,(s)}=0,1} P(C_\alpha^{(1)} + \partial v_\alpha^{(s)} + d_x^{\alpha,(s)}\gamma_x + d_y^{\alpha,(s)}\gamma_y) \right]. \quad (\text{A45})$$

As in (A14), the collection of terms in the bracket for each α can be mapped to the partition function of a $(n-1)$ -flavor RBIM:

$$\text{Tr}(\rho_{f,e}^n) = \frac{1}{4^{2n-2}} \left(\sqrt{(1-p_f)p_f} \right)^{(n-1)N} \left(\sqrt{(1-p_z)p_z} \right)^{(n-1)N} \overline{\left(Z_{p_f}^{\text{RBIM}}(J_f) \right)^{n-1}} \cdot \overline{\left(Z_{p_z}^{\text{RBIM}}(J_z) \right)^{n-1}}, \quad (\text{A46})$$

where J_α ($\alpha = z, f$) is the strength of Ising coupling for each of the two RBIMs. p_α denotes the probability of antiferromagnetic coupling on each bond. Both RBIMs are situated along the Nishimori line: $e^{-2J_\alpha} = \frac{p_\alpha}{1-p_\alpha}$. Again, the partition functions implicitly contain summations over the four boundary conditions. The von Neumann entropy can be obtained by taking the $n \rightarrow 1$ limit:

$$\begin{aligned} S(\rho_{f,e}) &= -\lim_{n \rightarrow 1} \frac{\partial}{\partial n} \text{Tr}(\rho_{f,e}) \\ &= -\log \overline{Z_{p_z}^{\text{RBIM}}(J_z)} - \log \overline{Z_{p_f}^{\text{RBIM}}(J_f)} + \left(-4 \log 2 - \frac{N}{2} \log[p_z(1-p_z)] - \frac{N}{2} \log[p_f(1-p_f)] \right), \end{aligned} \quad (\text{A47})$$

The terms in the parentheses is always regular for finite p_z, p_f , so we can focus on the first two terms, which is the free energy of two decoupled RBIMs. We denote the Ising spin variables of the two RBIMs as σ and τ , respectively. Then we can straightforwardly get the phase diagram of the statistical model, shown in Fig. 2.

Applying the same strategy as in section A, B, we can map the relative entropy and coherent information to observables in the RBIM. We directly list the results here.

1. Relative entropy. $D(\rho_{f,e} \parallel \rho_{f,e}^e)$ is mapped to the excess free energy of the defect line (connecting the inserted pair of e anyons) of the RBIM of spin σ ; $D(\rho_{f,e} \parallel \rho_{f,e}^f)$ is mapped to the excess free energy of the defect line (connecting the inserted pair of f anyons) of the RBIM of spin τ ; $D(\rho_{f,e} \parallel \rho_{f,e}^m)$ is mapped to the sum of the excess free energy of the defect line (connecting the inserted pair of m anyons) of the two RBIMs, because $w^m = w^e w^f$.

2. Coherent information,

$$I_c = 2 \log 2 - \log \left[\sum_{d_x, d_y=0,1} e^{-\Delta F_{d_x, d_y}^\sigma} \right] - \log \left[\sum_{d_x, d_y=0,1} e^{-\Delta F_{d_x, d_y}^\tau} \right], \quad (\text{A48})$$

where $\Delta F_{d_x, d_y}^{\sigma(\tau)}$ is the excess free energy of non-contractible defect lines in the RBIM of spin σ (τ). Across transitions at $p_z \approx 0.109$ and $p_f \approx 0.109$, I_c changes discontinuously. Quantum memory can only be realized when both σ and τ are in the FM phase, while classical memory corresponds to one of the spin species is in the FM phase while the other in the PM phase, and the topological memory is completely lost when both RBIMs are in the PM phase.

From the above mapping, we can relate the four phases of the RBIM to the four types of topological order (including the trivial one) in Fig. 2.

Appendix B: Exact solution to the gapless spin liquid phase of the toric code model through fermionization

In this section we analyze the properties the toric code model with additional ZX terms in the Hamiltonian,

$$H = -\sum_v A_v - \sum_p B_p - \sum_i h_{xz} Z_i X_{i+\delta}. \quad (\text{B1})$$

We show that this model can be solved exactly using the method introduced in [83]. Firstly, we note that the model has an extensive number of local conserved quantities. $[H, W_p] = 0$ with $W_p = A_{v=p-\delta} B_p$, which follows from the fact

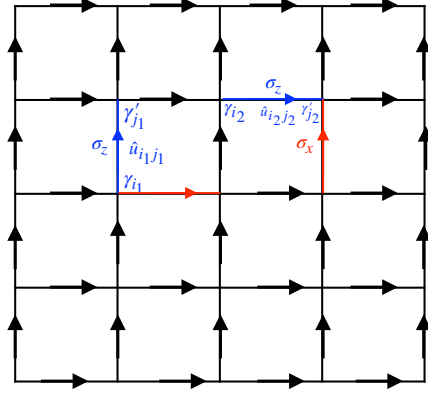


FIG. 10. The fermionization of the model in (B1). The links that Pauli matrices $Z_i, X_{i+\delta}$ act upon are colored in blue and red, respectively. There are two Majorana degrees of freedom $\gamma_{v_i}, \gamma'_{v_i}$ on each lattice site v_i in the fermionized Hilbert space, corresponding to the f anyon in the toric code model and we implicitly assume that the location of the f anyon is the same as the comprising e anyon. The term $Z_i X_{i+\delta}$ are fermionized as $i u_i \gamma_{v_i} \gamma'_{v'_i}$, where v_i, v'_i is the starting point and the end point of the link i , with the direction defined by the arrows, and u_i is a static Z_2 gauge field on link i , which accounts for the mutual semion statistics between f -anyons (fermions) and m -anyons (Z_2 flux).

that the e anyons and adjacent m anyons are always created or annihilated in pairs, so we can solve the model in each simultaneous eigenspace of W_p . Secondly, the role of ZX term is to induce pair creation, annihilation and hopping of f anyons, which are fermions. Then on a infinite lattice or a topologically trivial lattice, in each sector $\{W_p = w_p\}$, the only degrees of freedom are the f anyons, so we expect in each sector the model can be described by a fermion tight-binding model. We assume the fermions are defined on the vertices of the lattice, with the mapping

$$n_v^f \longleftrightarrow \frac{1 - A_v}{2}, \quad (\text{B2})$$

where $n_v^f = f_v^\dagger f_v$ is the fermion number operator. This mapping follows naturally from the observation that in the zero-flux sector $\{w_p = 1\}$, $\frac{1 - A_v}{2}$ corresponds to the occupation number of the f anyon on v . Finally, because f and e/m anyons are mutual semions, an f anyon can acquire a nontrivial phase depending on w_p when moving around the plaquette p . Thus W_p should correspond to static Z_2 flux on each plaquette in the fermion model, so we have the following mapping,

$$T_{v_i v'_i} \equiv i u_i \gamma_{v_i} \gamma'_{v'_i} \longleftrightarrow Z_i X_{i+\delta}, \quad \text{link } i \equiv \langle v_i v'_i \rangle \quad (\text{B3})$$

where $\gamma_v = f_v + f_v^\dagger, \gamma'_{v'} = -i(f_{v'} - f_{v'}^\dagger)$ are Majorana fermion operators and $u_i = \pm 1$ are static Z_2 gauge fields defined on links. It is straightforward to check that the commutation and anti-commutation relation between $Z_i X_{i+\delta}$ is preserved under the above mapping:

$$\begin{cases} \{T_{v_i v'_i}, T_{v_j v'_j}\} = 0, & \text{if } i = j \pm \delta \\ [T_{v_i v'_i}, T_{v_j v'_j}] = 0, & \text{otherwise} \end{cases} \longleftrightarrow \begin{cases} \{Z_i X_{i+\delta}, Z_j X_{j+\delta}\} = 0, & \text{if } i = j \pm \delta \\ [Z_i X_{i+\delta}, Z_j X_{j+\delta}] = 0, & \text{otherwise} \end{cases} \quad (\text{B4})$$

The commutation and anti-commutation relation between $Z_i X_{i+\delta}$ and A_v (and similarly for $B_p = A_{v=p-\delta} W_p$) is also preserved:

$$\begin{cases} \{T_{v_i v'_i}, 1 - 2n_v^f\} = 0, & \text{if } v \in \partial i \\ [T_{v_i v'_i}, 1 - 2n_v^f] = 0, & \text{otherwise} \end{cases} \longleftrightarrow \begin{cases} \{Z_i X_{i+\delta}, A_v\} = 0, & \text{if } v \in \partial i \\ [Z_i X_{i+\delta}, A_v] = 0, & \text{otherwise} \end{cases} \quad (\text{B5})$$

Besides, $Z_i X_{i+\delta}$ and A_v, B_p satisfy an additional relation:

$$\prod_{i \in \partial p} Z_i X_{i+\delta} = B_p A_{v=p+\delta}. \quad (\text{B6})$$

Under the mapping in (B3), the left hand side of (B6) is mapped to $\prod_{i \in \partial p} T_{v_i v'_i} = (1 - 2n_{p-\delta}^f)(1 - 2n_{p+\delta}^f) \prod_{i \in \partial p} \hat{u}_i$. The right hand side of (B6) can be rewritten as $W_p A_{p-\delta} A_{p+\delta}$. Then (B6) together with the (B2) determines the Z_2

flux configuration in the fermion model,

$$\prod_{i \in \partial p} \hat{u}_i \leftrightarrow A_{p-\delta} B_p = W_p, \quad (\text{B7})$$

as expected. (B2),(B3),(B7) form the complete the dictionary of the fermionization procedure on an infinite lattice or a topologically trivial lattice. However, on the fermionic side, under periodic boundary condition, i.e., on a torus, there are additional Z_2 fluxes threading the two non-contractible cycles γ_x, γ_y along the x, y direction: $\hat{w}_{x,y} = \prod_{i \in \gamma_{x,y}} \hat{u}_i$. We need to figure out what is the counterpart of $\hat{w}_{x,y}$ on the toric code side. This can be done by using again the mapping in (B3), which leads to

$$-\left(\prod_{i \in \gamma_{x,y}} \hat{u}_i \right) \prod_{i \in \gamma_{x,y}} (1 - 2n_{v_i}^f) \leftrightarrow \prod_{i \in \gamma_{x,y}} Z_i X_{i+\delta}. \quad (\text{B8})$$

By using (B2), we obtain,

$$-\hat{w}_{x(y)} \leftrightarrow \prod_{i \in \gamma_{x(y)}} A_{v_i} Z_i X_{i+\delta} = \prod_{i \in \gamma_{x(y)}} Z_i X_{i-\delta} \equiv \hat{W}_{\gamma_{x(y)}}^{f'}. \quad (\text{B9})$$

Indeed, $\hat{W}_{\gamma_x}^{f'}, \hat{W}_{\gamma_y}^{f'}$ are also conserved quantities in the original model, $[\hat{W}_{\gamma_{x(y)}}^{f'}, H] = 0$.

In the end, we map the model in (B1) to a quadratic fermion model with static Z_2 gauge field,

$$H \leftrightarrow \tilde{H} = \sum_v (2n_v^f - 1) \cdot (1 + \hat{w}_p) - h_{xz} \sum_{\langle vv' \rangle} i \hat{u}_{vv'} \gamma_v \gamma_{v'}, \quad (\text{B10})$$

where $\hat{w}_p = \prod_{\langle vv' \rangle \in \partial p} \hat{u}_{vv'}$.

Thanks to the extensive number of conserved quantities, $[\hat{u}_{vv'}, \tilde{H}] = [\hat{w}_p/x/y, \tilde{H}] = 0$, \tilde{H} can be reduced to a free fermion model in each Z_2 flux sector $\{\hat{w}_p = w_p, \hat{w}_x = w_x, \hat{w}_y = w_y\}$, and thus can be easily solved. In the case $h_{xz} = 0$, it is obvious that the ground state (the vacuum of f) lies in the zero flux sector $w_p = 1$, and the lowest energy state in the four sectors with distinct $\{w_x = \pm 1, w_y = \pm 1\}$ has degenerate eigenenergy. This is just another viewpoint of the well-known topological degeneracy.

Via numerical investigation we find that the ground state always stay in the sector with $w_p = 1$, irrespective of the value of h_{xz} , so we will mainly restrict our discussion to this case,

$$\tilde{H} = 4 \sum_v n_v^f - h_{xz} \sum_{\langle vv' \rangle} f_v^\dagger f_{v'} + f_v f_{v'} + h.c., \quad (\text{B11})$$

and $w_a = 1, -1 (a = x, y)$ corresponds to PBC and APBC along direction a , respectively. Then \tilde{H} can be solved via Fourier transformation, $f_v = \frac{1}{\sqrt{L_x L_y}} \sum_{k_a = \frac{2n_a \pi}{L_a}} f_k e^{ik_x v_x + ik_y v_y}$, where $n \in \mathbb{Z}$ for PBC and $n \in \mathbb{Z} + \frac{1}{2}$ for APBC,

$$\tilde{H} = \sum_k (f_k^\dagger, f_{-k}) \begin{pmatrix} 2 - h_{xz} (\cos k_x + \cos k_y) & -i h_{xz} (\sin k_x + \sin k_y) \\ i h_{xz} (\sin k_x + \sin k_y) & -2 + h_{xz} (\cos k_x + \cos k_y) \end{pmatrix} \begin{pmatrix} f_k \\ f_{-k}^\dagger \end{pmatrix}. \quad (\text{B12})$$

The dispersion of Bogoliubov quasiparticle excitation can be easily obtained,

$$\xi_k = \sqrt{[2 - h_{xz} (\cos k_x + \cos k_y)]^2 + [h_{xz} (\sin k_x + \sin k_y)]^2}, \quad (\text{B13})$$

and the ground state energy is $E_g = -\sum_k \xi_k$. For $h_{xz} < 1$, the spectrum is gapped and the ground energy is nearly degenerate (with an exponentially small splitting) for the 4 types of boundary conditions. This corresponds to the gapped topologically ordered phase of H . For $h_{xz} = 1$, the gap closes at $k_x = k_y = 0$, and remain closed for $h_{xz} > 1$, with linear dispersion at two Dirac points $k_x = -k_y = \pm \arccos \frac{1}{h_{xz}}$. So for $h_{xz} > 1$ the original model lies in a gapless spin liquid phase, reminiscent of the gapless phase of the Kitaev honeycomb model. In this phase the topological degeneracy is lifted by an algebraically small gap, but the ground state remains long-range entangle.

Appendix C: Details about the decohered Kitaev honeycomb model

1. The model

In this Appendix, we provide detailed analysis of the effect proliferation of the f anyons in the Kitaev honeycomb model at zero magnetic field:

$$H = -J_x \sum_{x\text{-bonds}} \sigma_j^x \sigma_k^x - J_y \sum_{y\text{-bonds}} \sigma_j^y \sigma_k^y - J_z \sum_{z\text{-bonds}} \sigma_j^z \sigma_k^z. \quad (\text{C1})$$

It can be exactly solved by introducing the Majorana fermion operators: $\sigma^\alpha = ib^\alpha b^0$. After fixing the Z_2 gauge fields as $\hat{u}_{jk} = ib_j^\alpha b_k^\alpha = 1$ (which corresponds to the zero gauge flux sector the ground state lies in), the Kitaev Hamiltonian (C1) becomes the following quadratic fermion model:

$$H_F = -J_x \sum_{x\text{-bonds}} b_j^x b_k^x - J_y \sum_{y\text{-bonds}} b_j^y b_k^y - J_z \sum_{z\text{-bonds}} b_j^z b_k^z, \quad (\text{C2})$$

whose ground state $|\psi_F\rangle$ can be easily solved. The physical ground state $|\Psi\rangle$ can be obtained by projection to the gauge invariant subspace using the projection operator $\hat{P} = \prod_i \frac{1+\hat{D}_i}{2}$, i.e., $|\Psi\rangle = \prod_i \frac{1+\hat{D}_i}{2} |\{u_{ij} = 1\}\rangle \otimes |\psi_F\rangle$, where $\hat{D}_i = b_i^x b_i^y b_i^z b_i^0$. We will focus on Abelian phase with $|J_z| > |J_x| + |J_y|$, where H_F is trivially gapped and $|\Psi\rangle$ belongs to the \mathbb{Z}_2 TO.

The effect of the noisy channel in (26) is to change the fermion part of the density matrix but leave the gauge field configuration invariant. This can be shown by writing the Kraus operators in terms of Majorana fermion operators: $\sigma_i^\alpha \sigma_j^\alpha = -i\hat{u}_{ij} b_i^0 b_j^0$. Thus the density matrix ρ_f can be written as:

$$\rho_f = \hat{P} |\{u_{ij} = 1\}\rangle \langle \{u_{ij} = 1\}| \otimes \rho_F \hat{P}, \quad (\text{C3})$$

where ρ_F is the Majorana fermion density matrix, which is $\rho_F = \mathcal{N}^{X,F} \circ \mathcal{N}^{Y,F} \circ \mathcal{N}^{Z,F} [\rho_{F,0}]$, where $\rho_{F,0} = |\psi_F\rangle \langle \psi_F|$ is the ground state of H_F . $\mathcal{N}^{\alpha,F} = \prod_{\langle ij \rangle} \mathcal{N}_{\langle ij \rangle}^{\alpha,F}$, with

$$\mathcal{N}_{\langle ij \rangle \in \alpha\text{-bonds}}^{\alpha,F} [\cdot] \equiv (1-p) \cdot + p b_i^0 b_j^0 \cdot b_j^0 b_i^0. \quad (\text{C4})$$

Similar to the case in the toric code model, we expect that the error-corrupted state ρ_f undergoes a phase transition in the mixed-state topological order at some critical error rate p_c . In the limit $|J_z| \gg |J_x|, |J_y|$, p_c can be determined by mapping to the RBIM, analogous to the case in the toric code, which gives $p_c \approx 0.109$. The topological quantum memory also breaks down to classical topological memory after the transition, with two remaining commuting logical operators:

$$W_{\gamma_x} = \prod_{\langle ij \rangle \in \gamma_x} \sigma_i^{\alpha(ij)} \sigma_j^{\alpha(ij)}, \quad W_{\gamma_y} = \prod_{\langle ij \rangle \in \gamma_y} \sigma_i^{\alpha(ij)} \sigma_j^{\alpha(ij)}, \quad (\text{C5})$$

where $\alpha_{\langle ij \rangle} = x, y, z$ for $\langle ij \rangle \in x\text{-bonds}, y\text{-bonds}, z\text{-bonds}$. The two logical operators are depicted in Fig.5. The residual classical memory is due to the fact that $[W_{\gamma_x}, \sigma_i^{\alpha(ij)} \sigma_j^{\alpha(ij)}] = [W_{\gamma_y}, \sigma_i^{\alpha(ij)} \sigma_j^{\alpha(ij)}] = 0, \forall \langle ij \rangle$.

2. Entanglement negativity

In this section, we compute the entanglement negativity of the ρ_f in the decohered Kitaev honeycomb model, starting from the Abelian phase. We will demonstrate the existence of nonzero TEN for any error rate p .

Again, we use the replica trick to compute the entanglement negativity:

$$\mathcal{E}_A(\rho_f) := \log \left\| \rho_f^{T_A} \right\|_1 = \lim_{2n \rightarrow 1} \frac{1}{2-2n} \log \frac{\text{Tr} \left(\rho_f^{T_A} \right)^{2n}}{\text{Tr} \rho_f^{2n}}. \quad (\text{C6})$$

First it is easy to show: $\lim_{2n \rightarrow 1} \text{Tr} \rho_f^{2n} = \text{Tr} \rho_f = 1$, due to the trace-preserving property of quantum channels. So we only need to deal with the numerator: $\text{Tr} \left(\rho_f^{T_A} \right)^{2n}$.

A general curve γ , which bipartites the honeycomb lattice into subregions A and $B = \bar{A}$, intersects the bonds of the honeycomb lattice. In order to partial transpose the degrees of freedom in A subregion, we should define new Z_2 gauge fields to replace the gauge fields on the intersected bonds. Following the notation in [110], we assume γ intersects $2L$ bonds, and we denote the bonds intersected by the curve γ as: $\langle a_n b_n \rangle, n = 1, 2, \dots, 2L$. If the Z_2 gauge field on the bonds $\langle a_{2n-1} b_{2n-1} \rangle$ and $\langle a_{2n} b_{2n} \rangle$ are $\hat{u}_{a_{2n-1} b_{2n-1}} = ib_{a_{2n-1}}^\alpha b_{b_{2n-1}}^\alpha, \hat{u}_{a_{2n} b_{2n}} = ib_{a_{2n}}^\beta b_{b_{2n}}^\beta$; then we introduce two Z_2 gauge fields in the A and B subregions respectively: $w_{A,n} = ib_{a_{2n-1}}^\alpha b_{a_{2n}}^\beta, w_{B,n} = ib_{b_{2n-1}}^\alpha b_{b_{2n}}^\beta$. Then the ground state configuration of the gauge fields on the intersected links can be written as:

$$|\{u_p\}\rangle = \frac{1}{\sqrt{2^L}} \sum_{w_A = w_B = \{\pm 1\}} |w_A, w_B\rangle, \quad (\text{C7})$$

where $\{|u_p\rangle\}$ is the direct product of $|u_{a_n b_n} = 1\rangle$. As a result, the ground state density matrix can be written as:

$$\rho_0 = \frac{1}{2^{N+L+1}} \sum_{g,g',w,w'} D_g |u_A, w\rangle |u_B, w\rangle \langle u_A, w' | \langle u_B, w' | \otimes \rho_{F,0} D_{g'}, \quad (\text{C8})$$

where the summation over g, g' is over all the possible sets of the lattice sites, and $D_g = \prod_{i \in g} D_i$. What's more, we can simply replace the $\rho_{F,0}$ with ρ_F to get the decohered density matrix ρ_f . The partial trace of the density matrix is:

$$\rho_f^{TA} = \frac{1}{2^{N+L+1}} \sum_{g,g',w,w'} D_{g'_A} D_{g_B} |u_A, w'\rangle |u_B, w\rangle \langle u_A, w | \langle u_B, w' | \otimes \rho_F^{TA} D_{g'_B} D_{g_A}. \quad (\text{C9})$$

Thus

$$\begin{aligned} (\rho_f^{TA})^2 &= \left(\frac{1}{2^{N+L+1}} \right)^2 \sum_{g,g',w,w'} \sum_{g_2,g'_2,w_2,w'_2} D_{g'_A} D_{g_B} [|u_A, w'\rangle |u_B, w\rangle \otimes \rho_F] \\ &\quad \langle u_A, w | \langle u_B, w' | D_{g'_B} D_{g_A} D_{g_2,B} D_{g'_2,A} |u_A, w'_2\rangle |u_B, w_2\rangle \\ &\quad \rho_F^{TA} \otimes \langle u_A, w_2 | \langle u_B, w'_2 |, \end{aligned} \quad (\text{C10})$$

where g_A, g_B , are the sets of lattice sites $g \cap A, g \cap B$, respectively. Now we split D_g into the gauge field part and fermion part: $D_g = X_g Y_g$, where $X_g = i^{|g|(|g|-1)/2} \prod_{j \in g} b_j^x b_j^y b_j^z$ and $Y_g = i^{|g|(|g|-1)/2} \prod_{j \in g} b_j^0$, where $|g|$ is the number of lattice sites in region g . The inner product can be simplified as:

$$\begin{aligned} &\langle u_A, w | \langle u_B, w' | D_{g'_B} D_{g_A} D_{g_2,B} D_{g'_2,A} |u_A, w'_2\rangle |u_B, w_2\rangle \\ &= \delta_{w,w'_2} \left(\delta_{g_A, g'_2, A} + x_A(w) \delta_{g_A, A-g'_2, A} Y_A \right) \delta_{w', w_2} \left(\delta_{g'_B, g_2, B} + x_A(w) \delta_{g'_B, B-g_2, B} Y_B \right) \\ &= \left(2\delta_{w,w'_2} P_{F,A}^{x_A(w)} \right) \left(2\delta_{w',w_2} P_{F,B}^{x_B(w')} \right), \end{aligned} \quad (\text{C11})$$

where $P_{F,A(B)}^x = \frac{1+xY_{A(B)}}{2}$ is the projection to the subspace with fixed Fermi parity x in subregion A (B), and $x_{A(B)}(w) = \langle u_{A(B)}, w | X_{A(B)} |u_{A(B)}, w\rangle = p_{A(B)} \prod_{n=1}^L w_n$, where we define $p_{A(B)} \equiv \prod_{i,j \in A(B)} u_{ij}$. Putting this inner product back into the $(\rho_f^{TA})^2$, we obtain:

$$\begin{aligned} (\rho_f^{TA})^2 &= \left(\frac{1}{2^{N+L+1}} \right)^2 \sum_{g,g',w,w'} D_g |u_A, w'\rangle |u_B, w\rangle \langle u_A, w' | \langle u_B, w | \otimes \rho_F^{TA} 2^N \left(2P_{F,A}^{x_A(w)} \right) \left(2P_{F,B}^{x_B(w')} \right) \rho_F^{TA} D_{g'} \\ &= \frac{1}{2^{N+2L}} \sum_{g,g',w,w'} D_g |u_A, w'\rangle |u_B, w\rangle \langle u_A, w' | \langle u_B, w | \otimes \rho_F^{TA} P_{F,A}^{x_A(w)} P_{F,B}^{x_B(w')} \rho_F^{TA} D_{g'} \end{aligned} \quad (\text{C12})$$

Now we move one step further to calculate $(\rho_f^{TA})^4$:

$$\begin{aligned} (\rho_f^{TA})^4 &= \left((\rho_f^{TA})^2 \right)^2 = \left(\frac{1}{2^{N+2L}} \right)^2 \sum_{g,g',w,w'} D_g |u_A, w'\rangle |u_B, w\rangle \langle u_A, w' | \langle u_B, w | \otimes \rho_F^{TA} P_{F,A}^{x_A(w)} P_{F,B}^{x_B(w')} \rho_F^{TA} D_{g'} \\ &\quad \sum_{g_2,g'_2,w_2,w'_2} D_{g_2} |u_A, w'_2\rangle |u_B, w_2\rangle \langle u_A, w'_2 | \langle u_B, w_2 | \otimes \rho_F^{TA} P_{F,A}^{x_A(w_2)} P_{F,B}^{x_B(w'_2)} \rho_F^{TA} D_{g'_2} \\ &= \left(\frac{1}{2^{N+2L}} \right)^2 \sum_{g,g',w,w'} D_g |u_A, w'\rangle |u_B, w\rangle \langle u_A, w' | \langle u_B, w | \otimes \rho_F^{TA} P_{F,A}^{x_A(w)} P_{F,B}^{x_B(w')} \rho_F^{TA} \\ &\quad 2^N \left(2P_{F,A}^{x_A(w')} \right) \left(2P_{F,B}^{x_B(w)} \right) \rho_F^{TA} P_{F,A}^{x_A(w)} P_{F,B}^{x_B(w')} \rho_F^{TA} D_{g'_2} \\ &= \frac{1}{2^{N+4L-2}} \sum_{g,g',w,w'} D_g |u_A, w'\rangle |u_B, w\rangle \langle u_A, w' | \langle u_B, w | \\ &\quad \otimes \left(\rho_F^{TA} P_{F,A}^{x_A(w)} P_{F,B}^{x_B(w')} \right) \left(\rho_F^{TA} P_{F,A}^{x_A(w')} P_{F,B}^{x_B(w)} \right) \left(\rho_F^{TA} P_{F,A}^{x_A(w)} P_{F,B}^{x_B(w')} \right) \rho_F^{TA} D_{g'}. \end{aligned} \quad (\text{C13})$$

With these results, we can now arrive at $(\rho_f^{TA})^{2n}$ by the iteration and induction:

$$\begin{aligned} (\rho_f^{TA})^{2n} &= \frac{1}{2^{N+2nL-2(n-1)}} \sum_{g,g',w,w'} D_g |u_A, w'\rangle |u_B, w\rangle \langle u_A, w' | \langle u_B, w | \\ &\quad \left[\left(\rho_F^{TA} P_{F,A}^{x_A(w)} P_{F,B}^{x_B(w')} \right) \left(\rho_F^{TA} P_{F,A}^{x_A(w')} P_{F,B}^{x_B(w)} \right) \right]^{n-1} \left(\rho_F^{TA} P_{F,A}^{x_A(w)} P_{F,B}^{x_B(w')} \right) D_{g'}. \end{aligned} \quad (\text{C14})$$

Using (C11) again, we can obtain the trace:

$$\begin{aligned} \text{Tr}(\rho_f^{T_A})^{2n} &= \frac{1}{2^{2nL-2n}} \sum_{w,w'} \text{Tr}_F \left(\rho_F^{T_A} P_{F,A}^{x_A(w')} P_{F,B}^{x_B(w)} \rho_F^{T_A} P_{F,A}^{x_A(w)} P_{F,B}^{x_B(w')} \right)^n \\ &= \frac{2^{L-1} \cdot 2^{L-1}}{2^{2n(L-1)}} \text{Tr}_F \left(\rho_F^{T_A} P_{F,A}^{p_A} P_{F,B}^{p_B} \rho_F^{T_A} P_{F,A}^{p_A} P_{F,B}^{p_B} + \rho_F^{T_A} P_{F,A}^{p_A} P_{F,B}^{-p_B} \rho_F^{T_A} P_{F,A}^{-p_A} P_{F,B}^{p_B} \right. \\ &\quad \left. + \rho_F^{T_A} P_{F,A}^{-p_A} P_{F,B}^{p_B} \rho_F^{T_A} P_{F,A}^{p_A} P_{F,B}^{-p_B} + \rho_F^{T_A} P_{F,A}^{-p_A} P_{F,B}^{-p_B} \rho_F^{T_A} P_{F,A}^{p_A} P_{F,B}^{-p_B} \right)^n \end{aligned} \quad (\text{C15})$$

Since the projector $D_{\text{tot}} = \prod_i D_i = X_{\text{tot}} Y_{\text{tot}} = 1$, the total fermion parity of the whole system is fixed by $Y_{\text{tot}} = X_{\text{tot}} = p_A p_B$. Therefore, terms in the bracket can be simplified as:

$$\begin{aligned} &\rho_F^{T_A} P_{F,A}^{p_A} P_{F,B}^{p_B} \rho_F^{T_A} P_{F,A}^{p_A} P_{F,B}^{p_B} + \rho_F^{T_A} P_{F,A}^{p_A} P_{F,B}^{-p_B} \rho_F^{T_A} P_{F,A}^{-p_A} P_{F,B}^{p_B} + \rho_F^{T_A} P_{F,A}^{-p_A} P_{F,B}^{p_B} \rho_F^{T_A} P_{F,A}^{p_A} P_{F,B}^{-p_B} + \rho_F^{T_A} P_{F,A}^{-p_A} P_{F,B}^{-p_B} \rho_F^{T_A} P_{F,A}^{p_A} P_{F,B}^{-p_B} \\ &= \rho_F^{T_A} (P_{F,A}^+ + P_{F,A}^-) (P_{F,B}^+ + P_{F,B}^-) \rho_F^{T_A} (P_{F,A}^+ + P_{F,A}^-) (P_{F,B}^+ + P_{F,B}^-) \\ &= (\rho_F^{T_A})^2 \end{aligned} \quad (\text{C16})$$

Then we can finally get the entanglement negativity:

$$\begin{aligned} \mathcal{E}_A(\rho_f) &= \log(\text{tr}(\rho_f^{T_A})) \\ &= \lim_{2n \rightarrow 1} \frac{1}{2-2n} \log \text{tr}(\rho_f^{T_A})^{2n} \\ &= L \log 2 - \log 2 + \log \|\rho_F^{T_A}\|_1, \end{aligned} \quad (\text{C17})$$

where the last term is the entanglement negativity $\varepsilon_A(\rho_F)$ of the density matrix of fermions. We note that the above result holds for any parameters J_x, J_y, J_z , and also for general bipartitions as long as the length of the boundary is even ($N_l = 2L$) and A, B are connected. To analyze the scaling behavior of ε_A , we again consider bipartition of a cylinder with translation invariant entanglement cut. In the gapped phase, $\rho_{F,0}$ is a Gaussian state with finite correlation length, so $\varepsilon_A(\rho_{F,0}) = \alpha L + \dots$ satisfies an area law with a vanishing subleading term for $L \rightarrow \infty$. We expect $\varepsilon_A(\rho_F)$ also have the same property after applying local channels on ρ_F , since local quantum channels cannot generate long-range entanglement. Thus we get $\text{TEN} = \log 2$, consistent with our expectation for even boundary sizes, which shows that this result holds for mixed-state topological order beyond stabilizer codes. For the decohered Kitaev honeycomb model, we still anticipate TEN to depend on the parity of N_l , like in the toric code model. Indeed, in the case $p = \frac{1}{2}$, ρ_f is equivalent to ρ_f up to an onsite unitary transformation. However, for general p , the calculation of negativity for odd N_l is more complicated and thus not shown here.

Appendix D: A proof that $e^2 m^2$ is a deconfined anyon

In this Appendix we prove that $e^2 m^2$ indeed becomes a deconfined anyon in the decohered double semion model, according to Definition 1. To start with, we write down the explicit form of the decohered state $\rho = \mathcal{N}^{[em]}[\rho_0]$, with maximal decoherence $p_0 = p_1 = p_2 = p_3 = \frac{1}{4}$. As discussed below (32), ρ is determined by the stabilizer group $G = \langle \{W_p^{e^3 m}\}, \text{nonlocal stabilizers} \rangle$,

$$\rho = \frac{1}{4^N} \sum_{g \in G} g. \quad (\text{D1})$$

We define the open $e^2 m^2$ string $W_{\tilde{C}}^{e^2 m^2} = \prod_{i \in \tilde{C}} X_i^2 Z_{i+\delta}^2$ on the dual lattice and $U_{\tilde{C}} = \frac{I + i W_{\tilde{C}}^{e^2 m^2}}{\sqrt{2}}$. Then $e^2 m^2$ anyons can be created at $\partial \tilde{C}$ by $\rho \rightarrow U_{\tilde{C}} \rho U_{\tilde{C}}^\dagger$. We prove below that both criteria in the definition of deconfined excitations are satisfied. The second criterion directly follows from the fact that $e^2 m^2$ anyons generate a strong 1-form symmetry of ρ , similar to the proof of the deconfinement of f anyons in Section III. The first criterion can be proved by contradiction. We assume that $e^2 m^2$ anyons can be locally created, i.e., $\exists V_{\partial \tilde{C}}$ supported near $\partial \tilde{C}$, s.t. $U_{\tilde{C}} \rho U_{\tilde{C}}^\dagger = V_{\partial \tilde{C}} \rho V_{\partial \tilde{C}}^\dagger$. Then we define two non-contractible Wilson loops $W_{\gamma_1}^e = \prod_{i \in \gamma_1} Z_i$, $W_{\gamma_2}^e = \prod_{i \in \gamma_2} Z_i^\dagger$, as depicted in Fig. 11. Because $W_{\gamma_1}^e W_{\gamma_2}^e$ commute with $V_{\partial \tilde{C}}$ as well as all the stabilizers, we have

$$W_{\gamma_1}^e W_{\gamma_2}^e V_{\partial \tilde{C}} \rho V_{\partial \tilde{C}}^\dagger W_{\gamma_1}^{e\dagger} W_{\gamma_2}^{e\dagger} = V_{\partial \tilde{C}} \rho V_{\partial \tilde{C}}^\dagger. \quad (\text{D2})$$

On the other hand, $W_{\gamma_1}^e W_{\gamma_2}^e$ anticommutes with $W_{\tilde{C}}^{e^2 m^2}$, so

$$W_{\gamma_1}^e W_{\gamma_2}^e U_{\tilde{C}} \rho U_{\tilde{C}}^\dagger W_{\gamma_1}^{e^\dagger} W_{\gamma_2}^{e^\dagger} = U_{\partial\tilde{C}}^\dagger \rho U_{\partial\tilde{C}} \neq U_{\tilde{C}} \rho U_{\tilde{C}}^\dagger, \quad (\text{D3})$$

which leads to contradiction with (D2). Therefore, $e^2 m^2$ cannot be locally created, so they are deconfined excitations in the decohered double semion model.

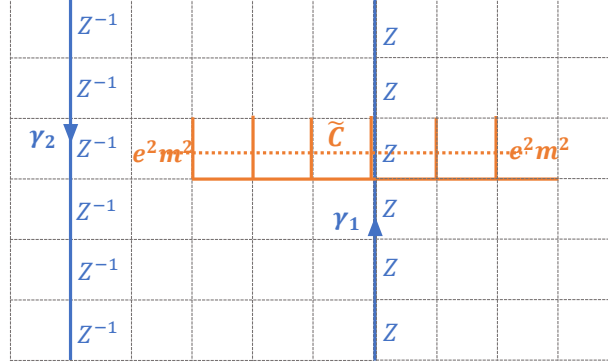


FIG. 11. Detecting $e^2 m^2$ anyons using Wilson loops.

-
- [1] X. G. WEN, “Topological orders in rigid states,” *International Journal of Modern Physics B* **04**, 239–271 (1990).
- [2] Xie Chen, Zheng-Cheng Gu, and Xiao-Gang Wen, “Local unitary transformation, long-range quantum entanglement, wave function renormalization, and topological order,” *Phys. Rev. B* **82**, 155138 (2010).
- [3] Xiao-Gang Wen, “Colloquium: Zoo of quantum-topological phases of matter,” *Rev. Mod. Phys.* **89**, 041004 (2017).
- [4] Lucile Savary and Leon Balents, “Quantum spin liquids: a review,” *Reports on Progress in Physics* **80**, 016502 (2016).
- [5] Yi Zhou, Kazushi Kanoda, and Tai-Kai Ng, “Quantum spin liquid states,” *Rev. Mod. Phys.* **89**, 025003 (2017).
- [6] Subir Sachdev, “Topological order, emergent gauge fields, and fermi surface reconstruction,” *Reports on Progress in Physics* **82**, 014001 (2018).
- [7] M. Aguado, G. K. Brennen, F. Verstraete, and J. I. Cirac, “Creation, manipulation, and detection of abelian and non-abelian anyons in optical lattices,” *Phys. Rev. Lett.* **101**, 260501 (2008).
- [8] Ruben Verresen, Mikhail D. Lukin, and Ashvin Vishwanath, “Prediction of toric code topological order from rydberg blockade,” *Phys. Rev. X* **11**, 031005 (2021).
- [9] Lorenzo Piroli, Georgios Styliaris, and J. Ignacio Cirac, “Quantum circuits assisted by local operations and classical communication: Transformations and phases of matter,” *Phys. Rev. Lett.* **127**, 220503 (2021).
- [10] Nathanan Tantivasadakarn, Ryan Thorngren, Ashvin Vishwanath, and Ruben Verresen, “Long-range entanglement from measuring symmetry-protected topological phases,” arXiv preprint arXiv:2112.01519 (2021).
- [11] Nathanan Tantivasadakarn, Ruben Verresen, and Ashvin Vishwanath, “The shortest route to non-abelian topological order on a quantum processor,” arXiv preprint arXiv:2209.03964 (2022).
- [12] Nathanan Tantivasadakarn, Ashvin Vishwanath, and Ruben Verresen, “Hierarchy of topological order from finite-depth unitaries, measurement, and feedforward,” *PRX Quantum* **4**, 020339 (2023).
- [13] Jong Yeon Lee, Wenjie Ji, Zhen Bi, and Matthew Fisher, “Decoding measurement-prepared quantum phases and transitions: from ising model to gauge theory, and beyond,” arXiv preprint arXiv:2208.11699 (2022).
- [14] Sergey Bravyi, Isaac Kim, Alexander Kliesch, and Robert Koenig, “Adaptive constant-depth circuits for manipulating non-abelian anyons,” arXiv preprint arXiv:2205.01933 (2022).
- [15] Tsung-Cheng Lu, Zhehao Zhang, Sagar Vijay, and Timothy H. Hsieh, “Mixed-state long-range order and criticality from measurement and feedback,” *PRX Quantum* **4**, 030318 (2023).
- [16] G. Semeghini *et al.*, “Probing topological spin liquids on a programmable quantum simulator,” *Science* **374**, 1242–1247 (2021).
- [17] K. J. Satzinger *et al.*, “Realizing topologically ordered states on a quantum processor,” *Science* **374**, 1237–1241 (2021).

- [18] T. I. Andersen *et al.*, “Non-abelian braiding of graph vertices in a superconducting processor,” *Nature* **618**, 264–269 (2023).
- [19] Shibo Xu *et al.*, “Digital simulation of projective non-abelian anyons with 68 superconducting qubits,” *Chinese Physics Letters* **40**, 060301 (2023).
- [20] Mohsin Iqbal *et al.*, “Topological order from measurements and feed-forward on a trapped ion quantum computer,” arXiv preprint arXiv:2302.01917 (2023).
- [21] Mohsin Iqbal *et al.*, “Creation of non-abelian topological order and anyons on a trapped-ion processor,” arXiv preprint arXiv:2305.03766 (2023).
- [22] John Preskill, “Quantum Computing in the NISQ era and beyond,” *Quantum* **2**, 79 (2018).
- [23] Eric Dennis, Alexei Kitaev, Andrew Landahl, and John Preskill, “Topological quantum memory,” *Journal of Mathematical Physics* **43**, 4452–4505 (2002).
- [24] H. Bombin, Ruben S. Andrist, Masayuki Ohzeki, Helmut G. Katzgraber, and M. A. Martin-Delgado, “Strong resilience of topological codes to depolarization,” *Phys. Rev. X* **2**, 021004 (2012).
- [25] Max McGinley and Nigel R. Cooper, “Fragility of time-reversal symmetry protected topological phases,” *Nature Physics* **16**, 1181–1183 (2020).
- [26] Tian-Shu Deng, Lei Pan, Yu Chen, and Hui Zhai, “Stability of time-reversal symmetry protected topological phases,” *Phys. Rev. Lett.* **127**, 086801 (2021).
- [27] Zijian Wang, Qiaoyi Li, Wei Li, and Zi Cai, “Symmetry-protected topological edge modes and emergent partial time-reversal symmetry breaking in open quantum many-body systems,” *Phys. Rev. Lett.* **126**, 237201 (2021).
- [28] Caroline de Groot, Alex Turzillo, and Norbert Schuch, “Symmetry Protected Topological Order in Open Quantum Systems,” *Quantum* **6**, 856 (2022).
- [29] Jong Yeon Lee, Yi-Zhuang You, and Cenke Xu, “Symmetry protected topological phases under decoherence,” arXiv preprint arXiv:2210.16323 (2022).
- [30] Jian-Hao Zhang, Yang Qi, and Zhen Bi, “Strange correlation function for average symmetry-protected topological phases,” arXiv preprint arXiv:2210.17485 (2022).
- [31] Ruihua Fan, Yimu Bao, Ehud Altman, and Ashvin Vishwanath, “Diagnostics of mixed-state topological order and breakdown of quantum memory,” arXiv preprint arXiv:2301.05689 (2023).
- [32] Yimu Bao, Ruihua Fan, Ashvin Vishwanath, and Ehud Altman, “Mixed-state topological order and the error-field double formulation of decoherence-induced transitions,” arXiv preprint arXiv:2301.05687 (2023).
- [33] Jong Yeon Lee, Chao-Ming Jian, and Cenke Xu, “Quantum criticality under decoherence or weak measurement,” arXiv preprint arXiv:2301.05238 (2023).
- [34] Ruochen Ma and Chong Wang, “Average symmetry-protected topological phases,” *Physical Review X* **13**, 031016 (2023).
- [35] Ruochen Ma, Jian-Hao Zhang, Zhen Bi, Meng Cheng, and Chong Wang, “Topological phases with average symmetries: the decohered, the disordered, and the intrinsic,” arXiv preprint arXiv:2305.16399 (2023).
- [36] Charles-Edouard Bardyn, Lukas Wawer, Alexander Altland, Michael Fleischhauer, and Sebastian Diehl, “Probing the topology of density matrices,” *Phys. Rev. X* **8**, 011035 (2018).
- [37] Liang Mao, Fan Yang, and Hui Zhai, “Dissipation dynamics driven transitions of the density matrix topology,” arXiv preprint arXiv:2301.04345 (2023).
- [38] Kaixiang Su, Nayan Myerson-Jain, Chong Wang, Chao-Ming Jian, and Cenke Xu, “Higher-form symmetries under weak measurement,” arXiv preprint arXiv:2304.14433 (2023).
- [39] Zijian Wang, Xu-Dong Dai, He-Ran Wang, and Zhong Wang, “Topologically ordered steady states in open quantum systems,” arXiv preprint arXiv:2306.12482 (2023).
- [40] Yu-Jie Liu and Simon Lieu, “Dissipative phase transitions and passive error correction,” *Phys. Rev. A* **109**, 022422 (2024).
- [41] F. A. Bais and J. K. Slingerland, “Condensate-induced transitions between topologically ordered phases,” *Phys. Rev. B* **79**, 045316 (2009).
- [42] Liang Kong, “Anyon condensation and tensor categories,” *Nuclear Physics B* **886**, 436–482 (2014), arXiv:1307.8244.
- [43] F.J. Burnell, “Anyon condensation and its applications,” *Annual Review of Condensed Matter Physics* **9**, 307–327 (2018).
- [44] P.W. Anderson, “Resonating valence bonds: A new kind of insulator?” *Materials Research Bulletin* **8**, 153–160 (1973).
- [45] N. Read and B. Chakraborty, “Statistics of the excitations of the resonating-valence-bond state,” *Phys. Rev. B* **40**, 7133–7140 (1989).
- [46] N. Read and Subir Sachdev, “Large- n expansion for frustrated quantum antiferromagnets,” *Phys. Rev. Lett.* **66**, 1773–1776 (1991).
- [47] X. G. Wen, “Mean-field theory of spin-liquid states with finite energy gap and topological orders,” *Phys. Rev. B* **44**, 2664–2672 (1991).
- [48] P. W. Anderson, “The resonating valence bond state in La_2CuO_4 and superconductivity,” *Science* **235**, 1196–1198 (1987).
- [49] T. Senthil and Matthew P. A. Fisher, “ \mathbb{Z}_2 gauge theory of electron fractionalization in strongly correlated systems,” *Phys. Rev. B* **62**, 7850–7881 (2000).
- [50] R. Moessner and S. L. Sondhi, “Resonating valence bond phase in the triangular lattice quantum dimer model,” *Phys. Rev. Lett.* **86**, 1881–1884 (2001).
- [51] A.Yu. Kitaev, “Fault-tolerant quantum computation by anyons,” *Annals of Physics* **303**, 2–30 (2003).
- [52] Eduardo Fradkin and Stephen H. Shenker, “Phase diagrams of lattice gauge theories with higgs fields,” *Phys. Rev. D* **19**, 3682–3697 (1979).
- [53] Yirun Arthur Lee and Guifre Vidal, “Entanglement negativity and topological order,” *Phys. Rev. A* **88**, 042318 (2013).
- [54] C. Castelnovo, “Negativity and topological order in the toric code,” *Phys. Rev. A* **88**, 042319 (2013).
- [55] Xueda Wen, Po-Yao Chang, and Shinsei Ryu, “Topological entanglement negativity in chern-simons theories,” *Journal of High Energy Physics* **2016**, 12 (2016).
- [56] Xueda Wen, Shunji Matsuura, and Shinsei Ryu, “Edge theory approach to topological entanglement entropy, mutual information, and entanglement negativity in chern-simons theories,” *Phys. Rev. B* **93**, 245140 (2016).
- [57] Alexei Kitaev and John Preskill, “Topological entanglement entropy,” *Phys. Rev. Lett.* **96**, 110404 (2006).
- [58] Michael Levin and Xiao-Gang Wen, “Detecting topological order in a ground state wave function,” *Phys. Rev.*

- Lett.* **96**, 110405 (2006).
- [59] O. Hart and C. Castelnuovo, “Entanglement negativity and sudden death in the toric code at finite temperature,” *Phys. Rev. B* **97**, 144410 (2018).
- [60] Tsung-Cheng Lu, Timothy H. Hsieh, and Tarun Grover, “Detecting topological order at finite temperature using entanglement negativity,” *Phys. Rev. Lett.* **125**, 116801 (2020).
- [61] Tsung-Cheng Lu, En-Jui Kuo, and Hung-Hwa Lin, “Entanglement cost in topological stabilizer models at finite temperature,” arXiv preprint arXiv:2201.08382 (2022).
- [62] Tsung-Cheng Lu and Sagar Vijay, “Characterizing long-range entanglement in a mixed state through an emergent order on the entangling surface,” arXiv preprint arXiv:2201.07792 (2022).
- [63] Davide Gaiotto, Anton Kapustin, Nathan Seiberg, and Brian Willett, “Generalized global symmetries,” *Journal of High Energy Physics* **2015**, 172 (2015).
- [64] Xiao-Gang Wen, “Emergent anomalous higher symmetries from topological order and from dynamical electromagnetic field in condensed matter systems,” *Phys. Rev. B* **99**, 205139 (2019).
- [65] John McGreevy, “Generalized symmetries in condensed matter,” *Annual Review of Condensed Matter Physics* **14**, 57–82 (2023).
- [66] Leonardo A Lessa, Meng Cheng, and Chong Wang, “Mixed-state quantum anomaly and multipartite entanglement,” arXiv preprint arXiv:2401.17357 (2024).
- [67] Benjamin Schumacher and M. A. Nielsen, “Quantum data processing and error correction,” *Phys. Rev. A* **54**, 2629–2635 (1996).
- [68] Benjamin Schumacher and Michael D. Westmoreland, “Approximate quantum error correction,” (2001), arXiv:quant-ph/0112106 [quant-ph].
- [69] Hidetoshi Nishimori, “Internal Energy, Specific Heat and Correlation Function of the Bond-Random Ising Model,” *Progress of Theoretical Physics* **66**, 1169–1181 (1981), <https://academic.oup.com/ptp/article-pdf/66/4/1169/5265369/66-4-1169.pdf>.
- [70] Asher Peres, “Separability criterion for density matrices,” *Phys. Rev. Lett.* **77**, 1413–1415 (1996).
- [71] Michał Horodecki, Paweł Horodecki, and Ryszard Horodecki, “Separability of mixed states: necessary and sufficient conditions,” *Physics Letters A* **223**, 1–8 (1996).
- [72] Karol Życzkowski, Paweł Horodecki, Anna Sanpera, and Maciej Lewenstein, “Volume of the set of separable states,” *Phys. Rev. A* **58**, 883–892 (1998).
- [73] G. Vidal and R. F. Werner, “Computable measure of entanglement,” *Phys. Rev. A* **65**, 032314 (2002).
- [74] Xiao-Gang Wen, “Quantum orders in an exact soluble model,” *Phys. Rev. Lett.* **90**, 016803 (2003).
- [75] Alexei Kitaev, “Anyons in an exactly solved model and beyond,” *Annals of Physics* **321**, 2–111 (2006), January Special Issue.
- [76] Claudio Castelnuovo and Claudio Chamon, “Topological order and topological entropy in classical systems,” *Phys. Rev. B* **76**, 174416 (2007).
- [77] Claudio Castelnuovo and Claudio Chamon, “Entanglement and topological entropy of the toric code at finite temperature,” *Phys. Rev. B* **76**, 184442 (2007).
- [78] Claudio Castelnuovo and Claudio Chamon, “Topological order in a three-dimensional toric code at finite temperature,” *Phys. Rev. B* **78**, 155120 (2008).
- [79] Simon Trebst, Philipp Werner, Matthias Troyer, Kirill Shtengel, and Chetan Nayak, “Breakdown of a topological phase: Quantum phase transition in a loop gas model with tension,” *Phys. Rev. Lett.* **98**, 070602 (2007).
- [80] I. S. Tupitsyn, A. Kitaev, N. V. Prokof’ev, and P. C. E. Stamp, “Topological multicritical point in the phase diagram of the toric code model and three-dimensional lattice gauge higgs model,” *Phys. Rev. B* **82**, 085114 (2010).
- [81] Sébastien Dusuel, Michael Kamfor, Román Orús, Kai Phillip Schmidt, and Julien Vidal, “Robustness of a perturbed topological phase,” *Phys. Rev. Lett.* **106**, 107203 (2011).
- [82] Andrés M. Somoza, Pablo Serna, and Adam Nahum, “Self-dual criticality in three-dimensional F_2 gauge theory with matter,” *Phys. Rev. X* **11**, 041008 (2021).
- [83] Yu-An Chen, Anton Kapustin, and Dorde Radicevic, “Exact bosonization in two spatial dimensions and a new class of lattice gauge theories,” *Annals of Physics* **393**, 234–253 (2018).
- [84] Eduardo Fradkin and Joel E. Moore, “Entanglement entropy of 2d conformal quantum critical points: Hearing the shape of a quantum drum,” *Phys. Rev. Lett.* **97**, 050404 (2006).
- [85] H. Casini, M. Huerta, and L. Leitao, “Entanglement entropy for a dirac fermion in three dimensions: Vertex contribution,” *Nuclear Physics B* **814**, 594–609 (2009).
- [86] Pablo Bueno, Robert C. Myers, and William Witczak-Krempa, “Universality of corner entanglement in conformal field theories,” *Phys. Rev. Lett.* **115**, 021602 (2015).
- [87] This equality always holds for contractible $\tilde{\gamma}$, while for non-contractible $\tilde{\gamma}$ it only holds for a particular choice of the initial state ρ_0 : $W_{\tilde{\gamma}}\rho_0 = \rho_0$. Fortunately, for the argument below we only need to use this condition for contractible $\tilde{\gamma}$, so this subtlety can be safely ignored.
- [88] Berislav Buca and Tomaz Prosen, “A note on symmetry reductions of the Lindblad equation: Transport in constrained open spin chains,” *New J. Phys.* **14**, 073007 (2012), arXiv:1203.0943 [quant-ph].
- [89] Simon Lieu, Ron Belyansky, Jeremy T. Young, Rex Lundgren, Victor V. Albert, and Alexey V. Gorshkov, “Symmetry breaking and error correction in open quantum systems,” *Phys. Rev. Lett.* **125**, 240405 (2020).
- [90] Michael Levin and Xiao-Gang Wen, “Fermions, strings, and gauge fields in lattice spin models,” *Phys. Rev. B* **67**, 245316 (2003).
- [91] Zijian Wang and Linhao Li, “Anomaly in open quantum systems and its implications on mixed-state quantum phases,” arXiv preprint arXiv:2403.14533 (2024).
- [92] This manuscript has been substantially revised since our first submission in July 2023. In the meantime, we became aware of two recent works [104, 105] on the same topic. The discussion regarding the non-modular anyon theory in Section IV B is inspired by these two works, where a connection between the intrinsic mixed-state TO and the topological subsystem code is established [102]. The perspective of 1-form symmetry anomaly is also adopted in another recent paper written by one of us [91].
- [93] Matthew B. Hastings, “Topological order at nonzero temperature,” *Phys. Rev. Lett.* **107**, 210501 (2011).

- [94] Shengqi Sang, Yijian Zou, and Timothy H Hsieh, “Mixed-state quantum phases: Renormalization and quantum error correction,” arXiv preprint arXiv:2310.08639 (2023).
- [95] John Watrous, *The theory of quantum information* (Cambridge university press, 2018).
- [96] Michael Levin and Zheng-Cheng Gu, “Braiding statistics approach to symmetry-protected topological phases,” *Phys. Rev. B* **86**, 115109 (2012).
- [97] Michael Levin, “Protected edge modes without symmetry,” *Phys. Rev. X* **3**, 021009 (2013).
- [98] Ruizhi Liu, Ho Tat Lam, Han Ma, and Liujun Zou, “Symmetries and anomalies of Kitaev spin-S models: Identifying symmetry-enforced exotic quantum matter,” *SciPost Phys.* **16**, 100 (2024).
- [99] Kyusung Hwang, “Mixed-state quantum spin liquid in kitaev lindbladian: Dynamical anyon condensation,” arXiv preprint arXiv:2305.09197 (2023).
- [100] Michael A. Levin and Xiao-Gang Wen, “String-net condensation: A physical mechanism for topological phases,” *Phys. Rev. B* **71**, 045110 (2005).
- [101] Tyler D. Ellison, Yu-An Chen, Arpit Dua, Wilbur Shirley, Nathanan Tantivasadakarn, and Dominic J. Williamson, “Pauli stabilizer models of twisted quantum doubles,” *PRX Quantum* **3**, 010353 (2022).
- [102] Tyler D. Ellison, Yu-An Chen, Arpit Dua, Wilbur Shirley, Nathanan Tantivasadakarn, and Dominic J. Williamson, “Pauli topological subsystem codes from Abelian anyon theories,” *Quantum* **7**, 1137 (2023).
- [103] Liang Kong and Xiao-Gang Wen, “Braided fusion categories, gravitational anomalies, and the mathematical framework for topological orders in any dimensions,” arXiv preprint arXiv:1405.5858 (2014).
- [104] Ramanjit Sohal and Abhinav Prem, “A noisy approach to intrinsically mixed-state topological order,” arXiv preprint arXiv:2403.13879 (2024).
- [105] Tyler Ellison and Meng Cheng, “Towards a classification of mixed-state topological orders in two dimensions,” arXiv preprint arXiv:2405.02390 (2024).
- [106] For convenience, we drop the subscript of p_f in Appendix A 1 to A 4.
- [107] Klaus Fredenhagen and Mihail Marcu, “Charged states in z_2 gauge theories,” *Communications in Mathematical Physics* **92**, 81–119 (1983).
- [108] K Gregor, David A Huse, R Moessner, and S L Sondhi, “Diagnosing deconfinement and topological order,” *New Journal of Physics* **13**, 025009 (2011).
- [109] Peng Rao and Inti Sodemann, “Theory of weak symmetry breaking of translations in F_2 topologically ordered states and its relation to topological superconductivity from an exact lattice z_2 charge-flux attachment,” *Phys. Rev. Res.* **3**, 023120 (2021).
- [110] Hong Yao and Xiao-Liang Qi, “Entanglement entropy and entanglement spectrum of the kitaev model,” *Phys. Rev. Lett.* **105**, 080501 (2010).